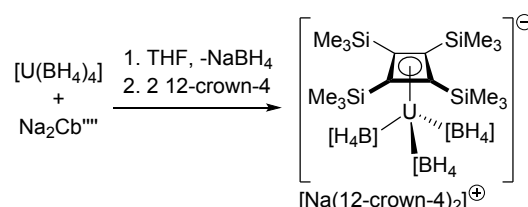


General Considerations

All manipulations were carried out using glovebox or standard Schlenk techniques. All glassware and cannulas were dried at 160°C overnight prior to use. Toluene and high boiling hydrocarbons were dried over molten potassium, distilled under a nitrogen atmosphere and stored in ampoules over a potassium mirror. Low boiling hydrocarbons were dried over sodium-potassium alloy, distilled under nitrogen and stored in ampoules over a potassium mirror. Deuterated toluene and THF were degassed by three freeze-thaw cycles, dried by refluxing over molten potassium for three days, vacuum distilled and stored in ampoules over 4 Å molecular sieves. $U(BH_4)_4$ was prepared as previously described.¹ $[Na_2Cb^{IV}(0.75.THF)]$ and $[K_2Cb^{IV}]$ were prepared according to literature procedures.²⁻⁴ 1H , $^{29}Si\{^1H\}$, $^{23}Na\{^1H\}$ and $^{11}B\{^1H\}$ NMR spectra were recorded on a Varian VNMR S400 spectrometer operating at 400 MHz (1H) and 30°C unless otherwise stated. The spectra were referenced internally to the residual protic solvent (1H). $^{29}Si\{^1H\}$ NMR spectra were referenced externally relative to $SiMe_4$, $^{23}Na\{^1H\}$ NMR spectra were referenced externally relative to a 0.1 M solution of NaCl in D_2O and $^{11}B\{^1H\}$ NMR spectra relative to $BF_3.OEt_2$. HR-ESI mass spectra were recorded on a Bruker FTICR-MS instrument in negative mode as THF solutions of the analyte at the University of Sussex. IR spectra were recorded on a Perkin Elmer 100 instrument as thin films between NaCl plates. Elemental analyses were performed by Microanalytisches Labor Pascher, Germany.

Synthesis of $[U(\eta^4-Cb^{IV})(BH_4)_3Na(THF)_3]$ and $[Na(12-crown-4)_2][U(\eta^4-Cb^{IV})(BH_4)_3]$



A Young's NMR tube was charged with $U(BH_4)_4$ (24 mg, 0.08 mmol), C_7D_8 (ca. 0.1-0.2 ml) and a few drops of THF- D_8 to produce a pale green solution. To this was added a solution of $Na_2Cb^{IV}(0.75.THF)$ (35.5 mg, 0.08 mmol) in THF- D_8 (ca 0.4 ml), which immediately produced a brown-red solution. The solution was filtered through a microfibre packed pipette and the solvent removed under a stream of argon to yield a brown microcrystalline solid, which was dissolved in Et_2O and filtered. The solvent was removed under a stream of argon and the residue was re-dissolved in THF (ca 2 ml). To this, *n*-heptane (4 ml) was added and the volume of the solution was reduced under a stream of argon until a crystalline solid started forming. The solution was then stored at $-35^\circ C$ overnight, yielding a microcrystalline solid. Yield: 50 mg (ca 67%).

NMR spectra were recorded in THF- D_8 . 1H NMR (δ/ppm): -5.12 (s, 36H, $SiMe_3$), 15.56 (s br., 12H, BH_4); $^{29}Si\{^1H\}$ NMR (δ/ppm): -208.4 (s, $SiMe_3$); $^{11}B\{^1H\}$ NMR (δ/ppm): 124.69 (s, BH_4 $\Delta\nu_{1/2} = 111$ Hz, no coupling to hydrogen observed in the ^{11}B -NMR spectrum); $^{23}Na\{^1H\}$ NMR (δ/ppm): -2.88 (s, $\Delta\nu_{1/2} = 29$ Hz); IR (thin film, cm^{-1}): 2475, 2427, 2302.4, 2202, 2138.6 ν_{BH} . Elemental analysis: found C 38.74, H 8.88; calculated for $[U(\eta^4-Cb^{IV})(BH_4)_3Na(THF)_3]$ ($C_{28}H_{72}B_3NaO_3Si_4U$) C 38.98, H 8.41.

The microcrystalline nature of $[U(\eta^4-Cb^{IV})(BH_4)_3Na(THF)_3]$ precluded structural characterization by X-ray crystallography. However, crystals suitable for single-crystal X-ray diffraction were obtained by adding 12-crown-4 (8.7 μl , 54 μmol) to a solution of $[U(\eta^4-Cb^{IV})(BH_4)_3Na(THF)_3]$ (23 mg) in $tBuOMe$ (1.5 ml), which resulted in the immediate precipitation of a brown microcrystalline material. The nascent solution was decanted away and the material was dried under a stream of argon and dissolved in a 1:1 THF/hexane mixture (2 ml), followed by slow evaporation of the solvent overnight, which resulted in the formation of brown-red plates of $[Na(12-crown-4)_2][U(\eta^4-Cb^{IV})(BH_4)_3]$. Crystals suitable for single-crystal X-ray diffraction were grown by slow evaporation of solvent from 1:1 THF/dioxane solution of the product at room temperature. Elemental analysis: Found C 38.02, H 7.77; Calculated for $[Na(12-crown-4)_2][U(\eta^4-Cb^{IV})(BH_4)_3]$ ($C_{32}H_{80}B_3NaO_8Si_4U$): C 38.48, H 8.07.

The only differences in the NMR spectra of $[U(\eta^4-Cb^{IV})(BH_4)_3Na(THF)_3]$ and $[Na(12-crown-4)_2][U(\eta^4-Cb^{IV})(BH_4)_3]$ in THF- D_8 were the observation of a singlet corresponding to 12-crown-4 at 4.77 ppm (32H) in

the ^1H NMR spectrum and a small downfield shift in the $^{23}\text{Na}\{^1\text{H}\}$ -NMR spectrum to -1.51 ppm ($\Delta\nu_{1/2} = 8.3$ Hz). The $^{29}\text{Si}\{^1\text{H}\}$ -NMR and $^{11}\text{B}\{^1\text{H}\}$ -NMR are unchanged. See Figures S6-S9.

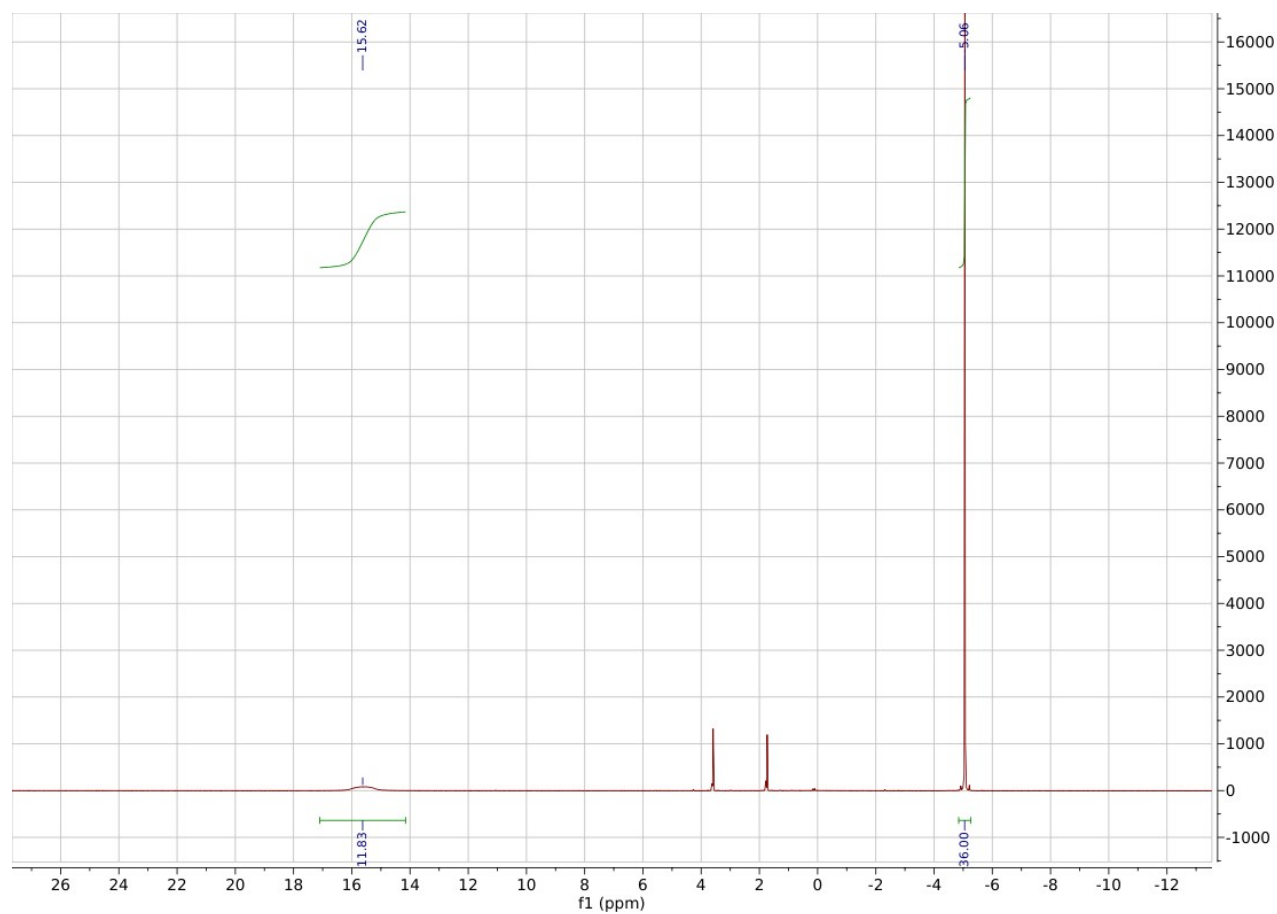


Figure S1. ^1H -NMR spectrum of $[\text{U}(\eta^4\text{-Cb''''})(\text{BH}_4)_3\text{Na}(\text{THF})_3]$ in THF-D_8 .

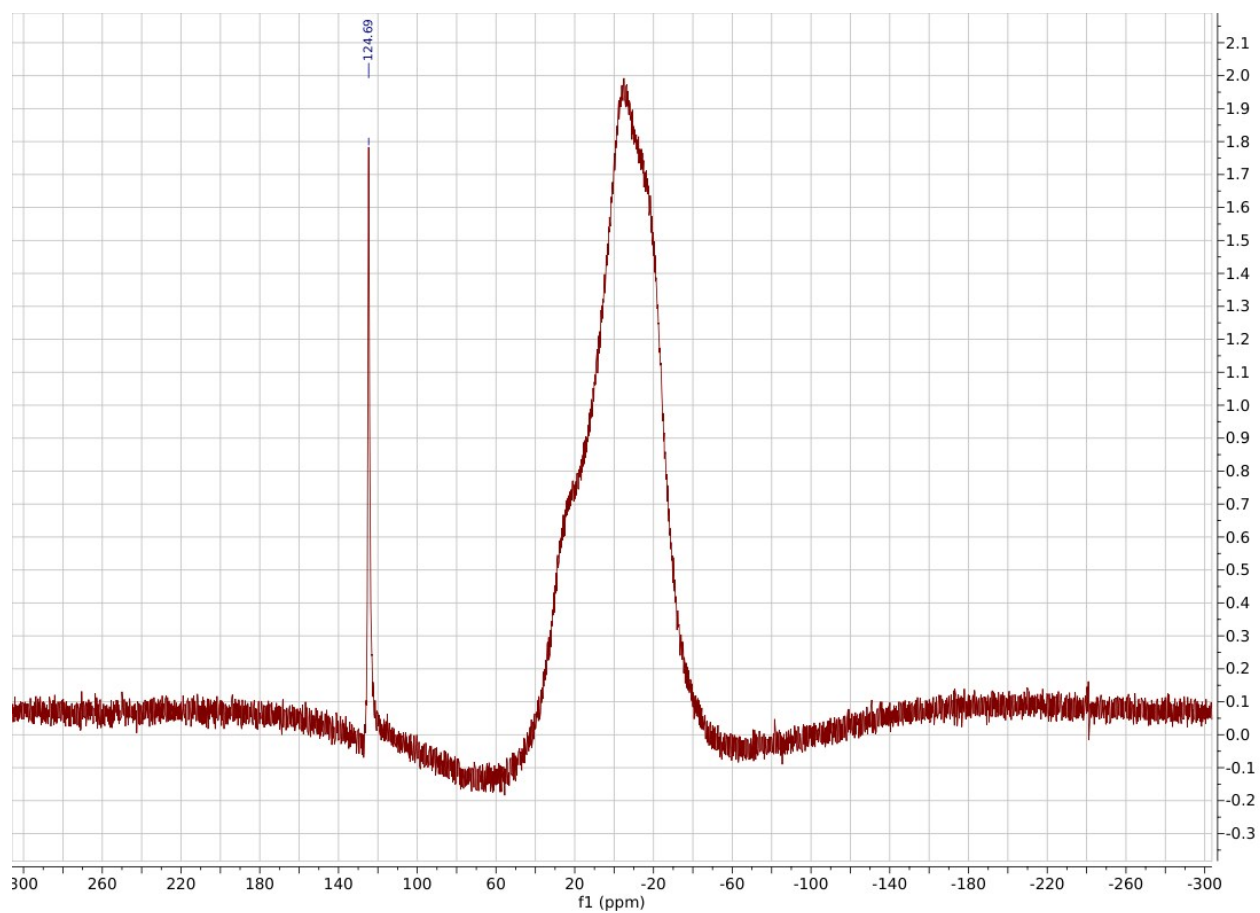


Figure S2. $^{11}\text{B}\{^1\text{H}\}$ NMR spectrum of $[\text{U}(\eta^4\text{-Cb}''''\text{)}(\text{BH}_4)_3\text{Na}(\text{THF})_3]$ in THF-D_8 .

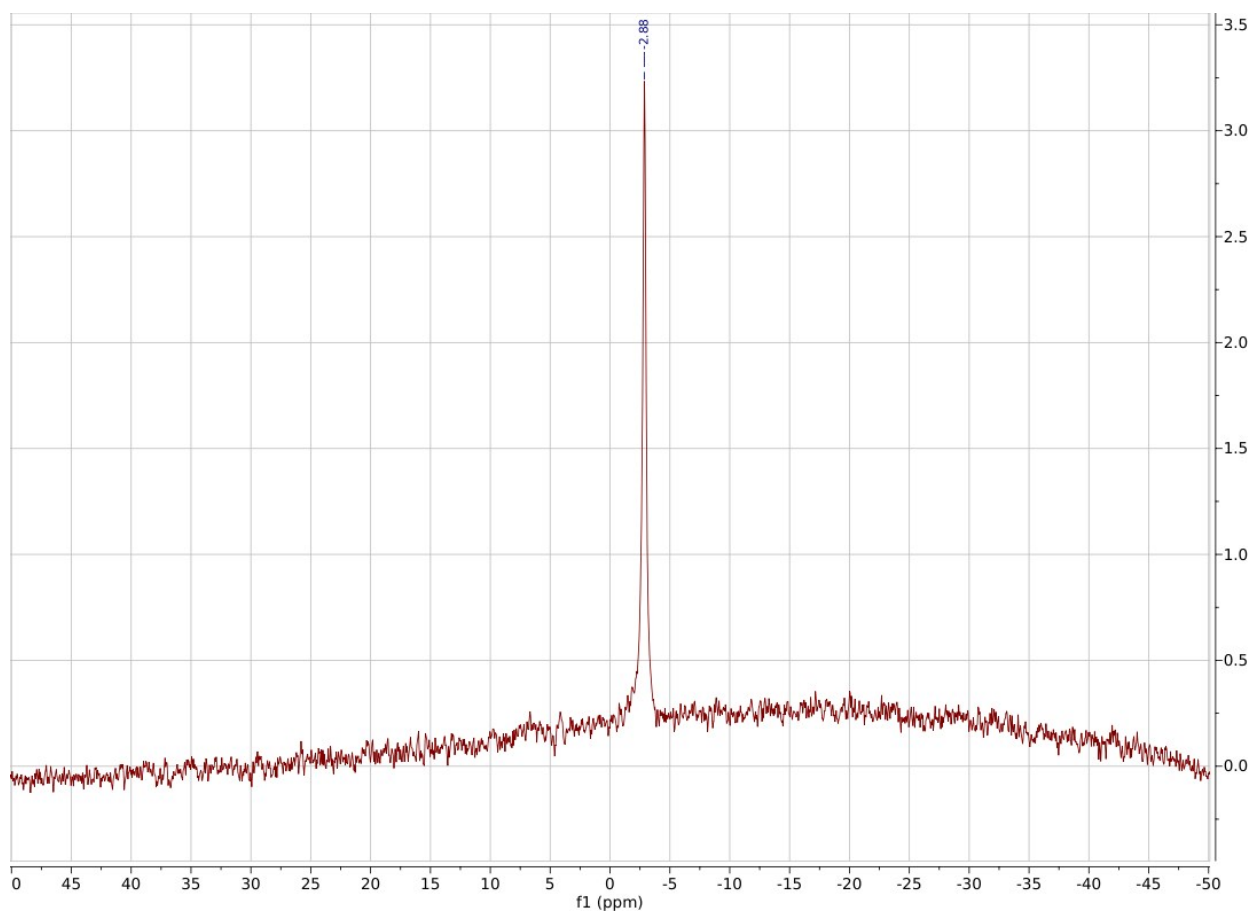


Figure S3. $^{23}\text{Na}\{^1\text{H}\}$ NMR spectrum of $[\text{U}(\eta^4\text{-Cb''''})(\text{BH}_4)_3\text{Na}(\text{THF})_3]$ in THF-D_8 .

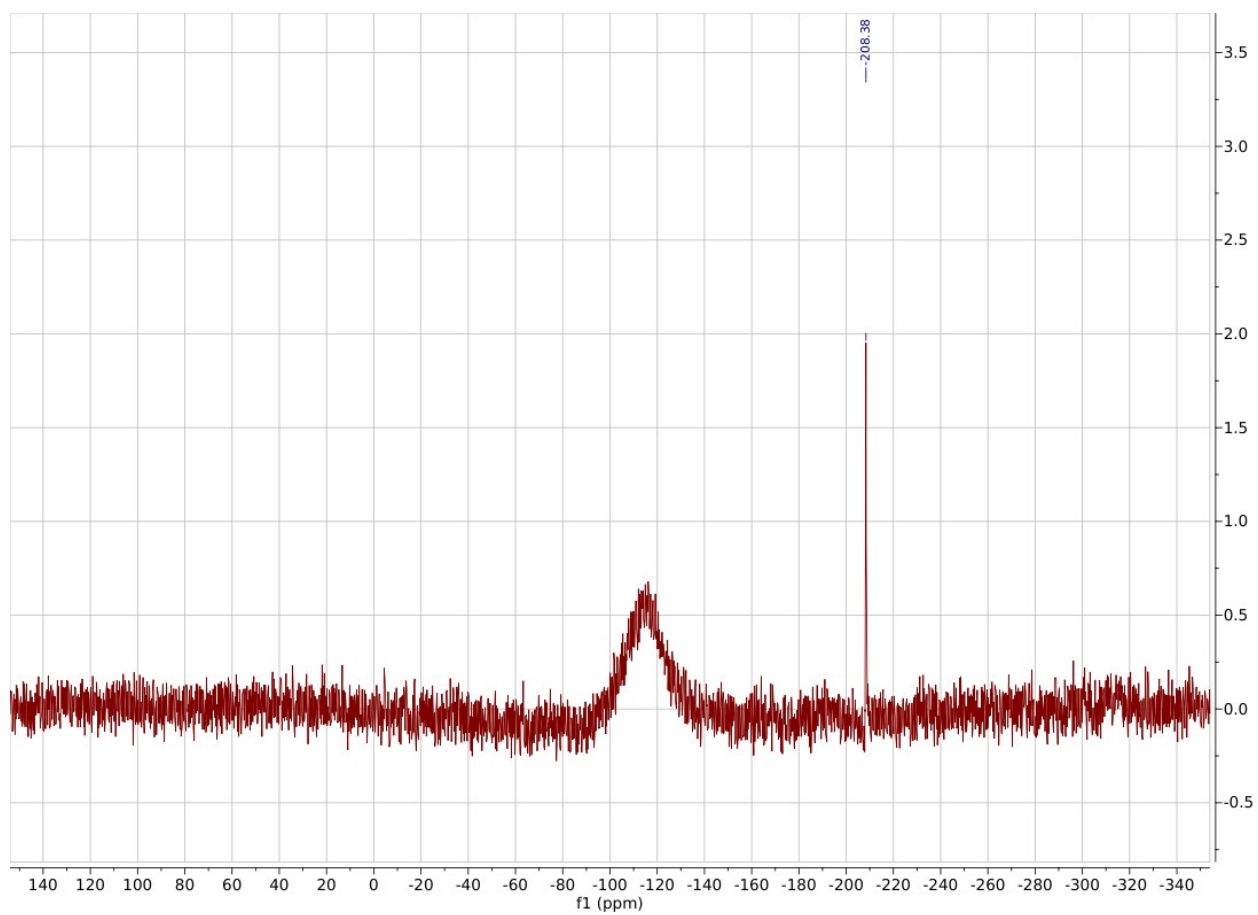


Figure S4. $^{29}\text{Si}\{^1\text{H}\}$ NMR spectrum of $[\text{U}(\eta^4\text{-Cb})(\text{BH}_4)_3\text{Na}(\text{THF})_3]$ in THF-D_8 .

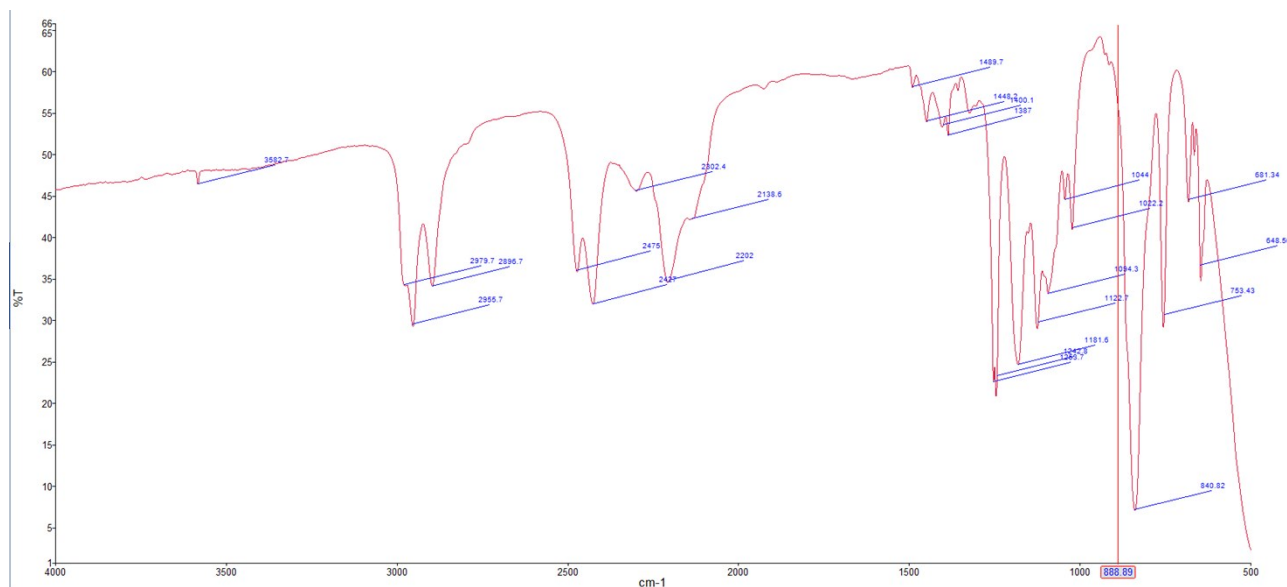


Figure S5. IR spectrum of $[\text{U}(\eta^4\text{-Cb''''})(\text{BH}_4)_3\text{Na}(\text{THF})_3]$.

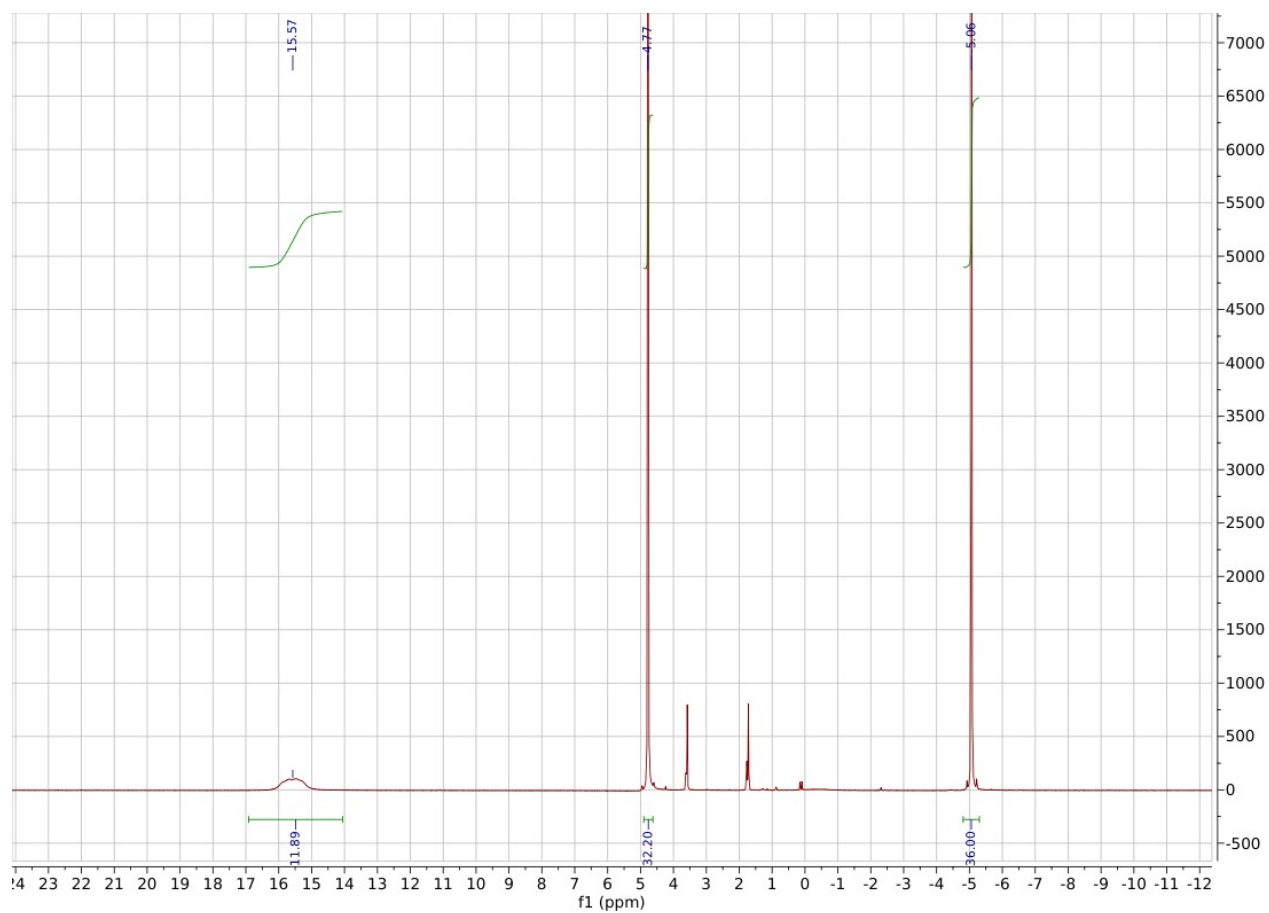


Figure S6. $^1\text{H-NMR}$ spectrum of $[\text{Na}(\text{12-crown-4})_2][\text{U}(\eta^4\text{-Cb}''')(\text{BH}_4)_3]$ in THF-D_8 .

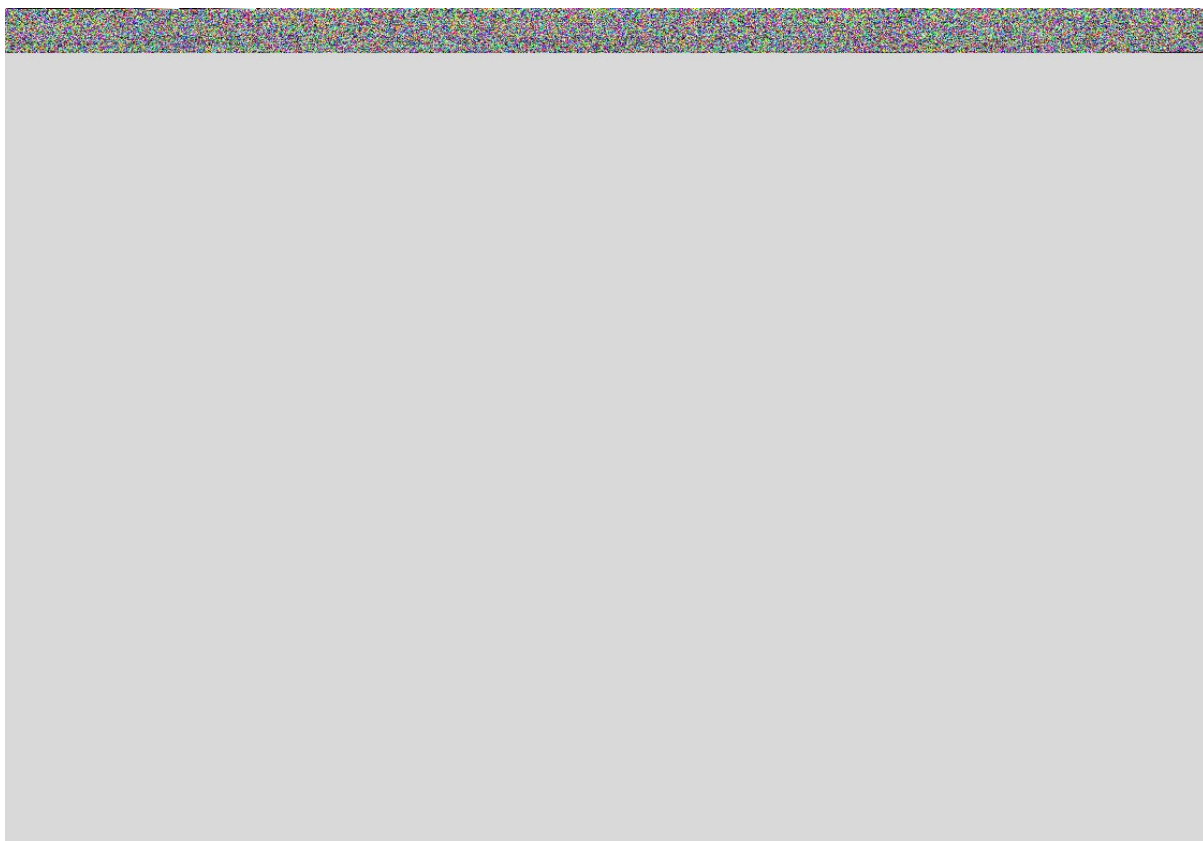


Figure S7. $^{11}\text{B}\{^1\text{H}\}$ NMR spectrum of $[\text{Na}(12\text{-crown-}4)_2][\text{U}(\eta^4\text{-Cb}''''\text{)}(\text{BH}_4)_3]$ in THF-D_8 .

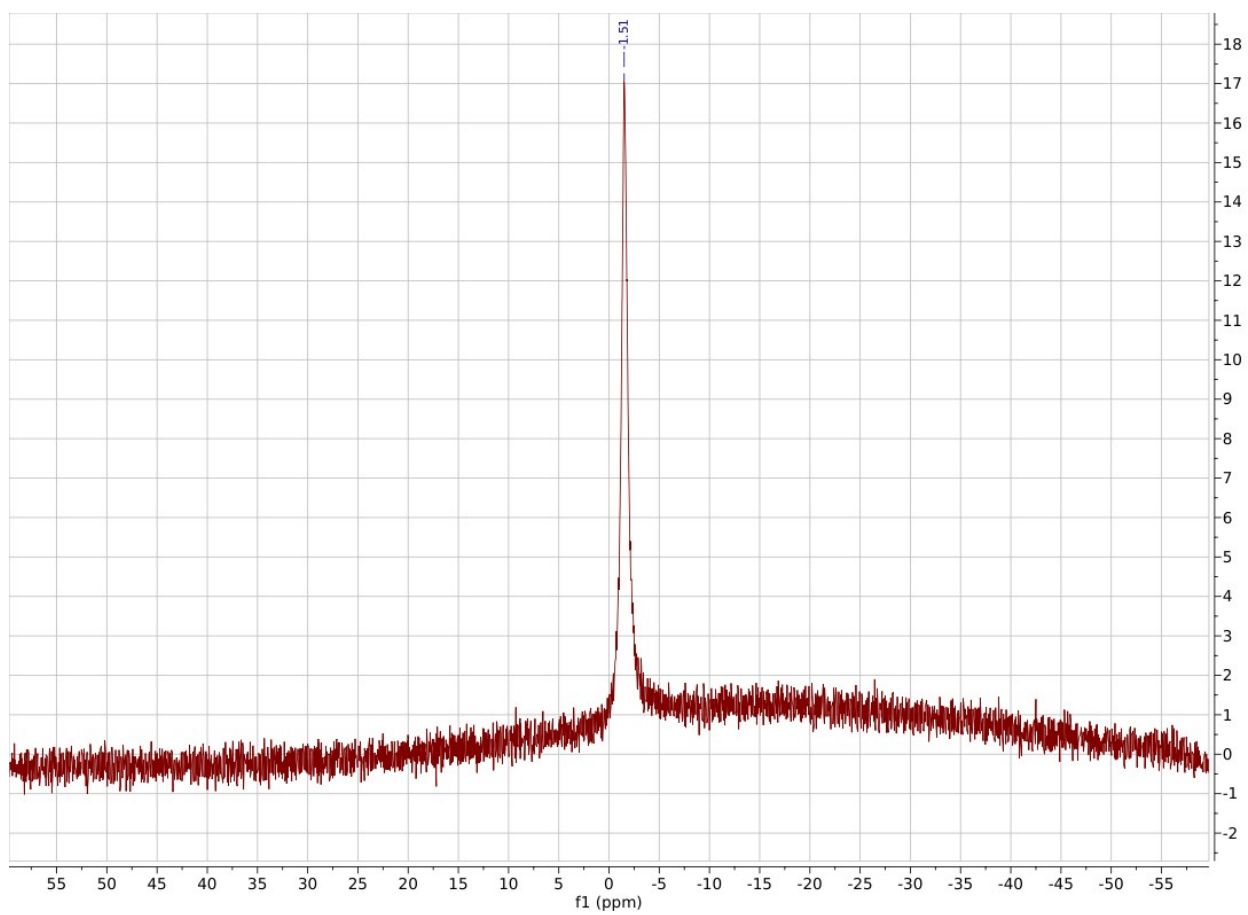


Figure S8. $^{23}\text{Na}\{^1\text{H}\}$ NMR spectrum of $[\text{Na}(12\text{-crown-4})_2][\text{U}(\eta^4\text{-Cb'''})(\text{BH}_4)_3]$ in THF-D_8 .

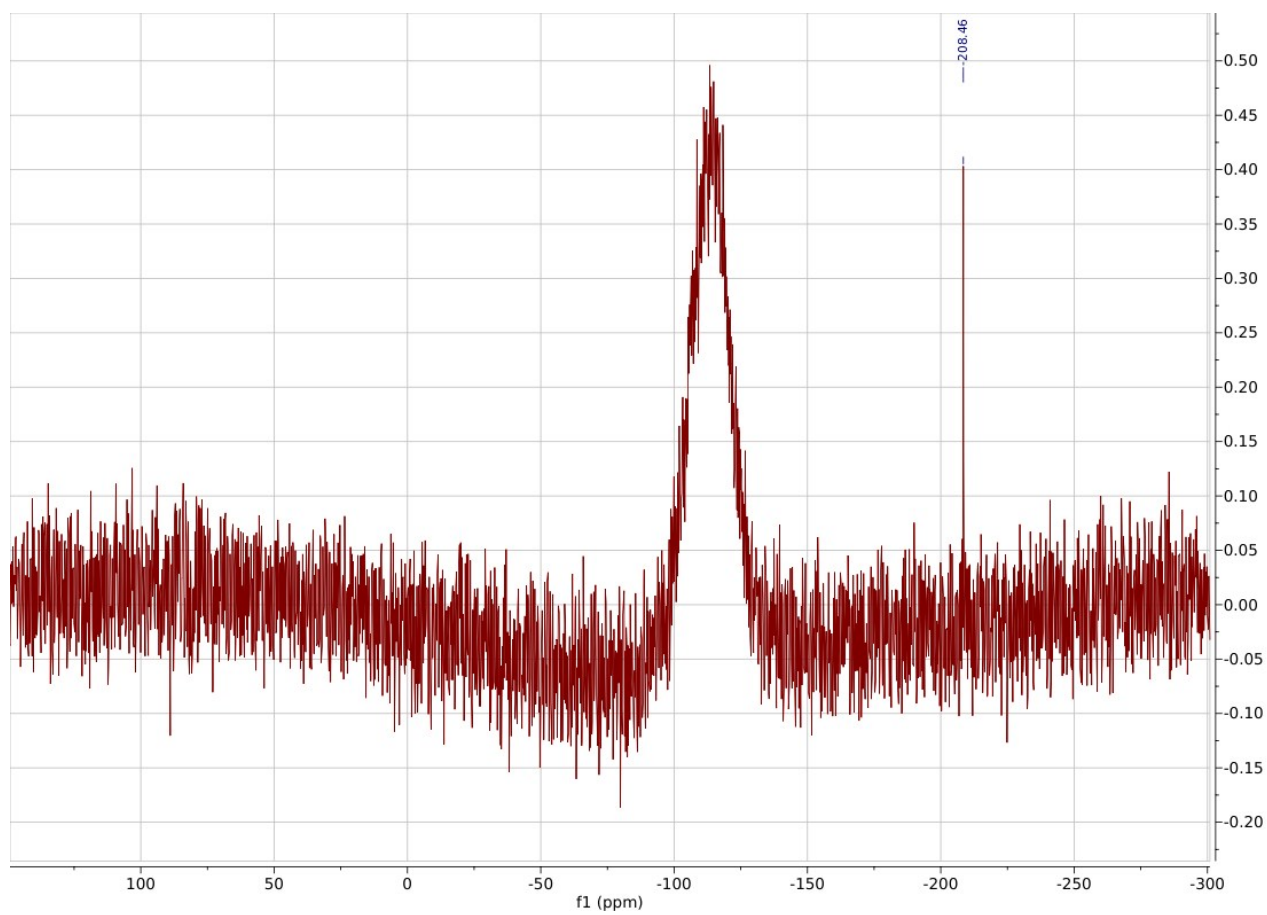


Figure S9. $^{29}\text{Si}\{^1\text{H}\}$ NMR spectrum of $[\text{Na}(12\text{-crown-}4)_2][\text{U}(\eta^4\text{-Cb})(\text{BH}_4)_3]$ in THF-D_8 .

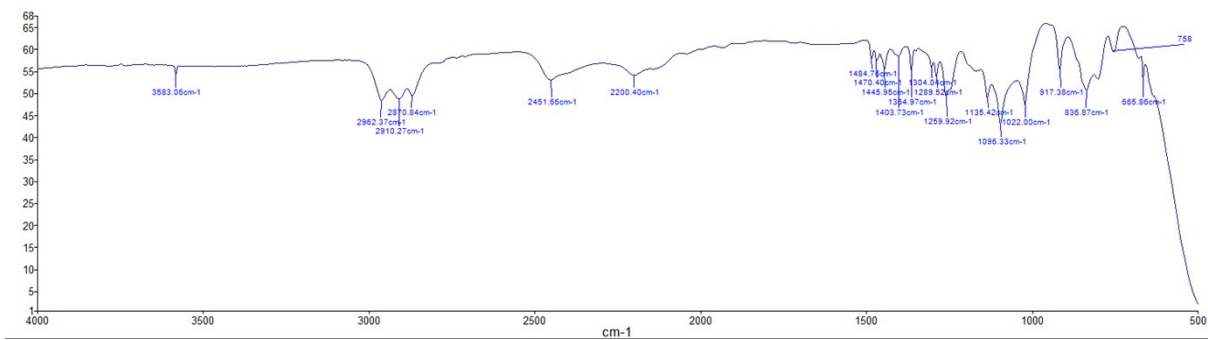
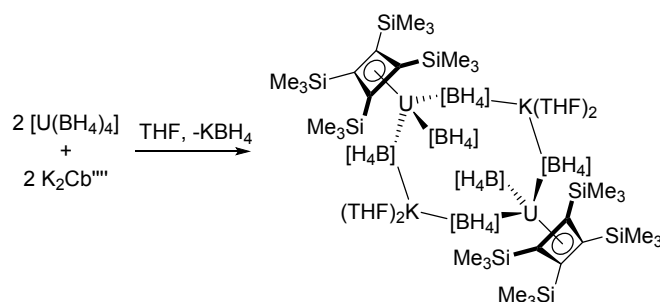


Figure S10. IR spectrum of $[\text{Na}(\text{12-crown-4})_2][\text{U}(\eta^4\text{-Cb'''})(\text{BH}_4)_3]$.

Synthesis of $[\text{U}(\eta^4\text{-Cb}''')(\mu\text{-BH}_4)_3\{\text{K}(\text{THF})_2\}]_2$



The synthesis of $[\text{U}(\eta^4\text{-Cb}''')(\mu\text{-BH}_4)_3\{\text{K}(\text{THF})_2\}]_2$ was accomplished in a similar manner to that described for $[\text{U}(\eta^4\text{-Cb}''')(\text{BH}_4)_3][\text{Na}(\text{THF})_4]$ using $\text{U}(\text{BH}_4)_4$ (30 mg, 0.1 mmol) and $\text{K}_2\text{Cb}'''$ (42 mg, 0.1 mmol) in a 2:1 mixture of THF- D_8 and toluene- D_8 (0.6 ml). After filtration, the solvent was removed under vacuum, the brown residue was dried, extracted into pentane (10 ml) and filtered again. The resulting brown solution was reduced in volume to *ca* 3 ml using a stream of argon, filtered again and the solvent volume reduced by slow evaporation to almost half, followed by storage at -35°C overnight. A crop (*ca* 10 mg) of brown crystals suitable for X-ray diffraction was obtained. The supernatant was decanted away and the residue washed with cold SiMe_4 (2×1 ml) and the washing combined with the mother-liquor, which resulted in the formation of a second crop of crystals. Total yield 40 mg, 21 %. The low isolated yield is due to the limited solubility of the compound in saturated hydrocarbons.

NMR spectra were recorded in THF- D_8 . ^1H NMR (δ/ppm): -4.87 (s, 36H, SiMe_3), 15.64 (s br., 12H, BH_4); $^{29}\text{Si}\{^1\text{H}\}$ -NMR (δ $\text{C}_4\text{D}_8\text{O}$): -208.3 (s, SiMe_3); $^{11}\text{B}\{^1\text{H}\}$ -NMR (δ $\text{C}_4\text{D}_8\text{O}$): 125.7 (s, BH_4 $\Delta\nu_{1/2} = 66.8$ Hz, no coupling to hydrogen was observed in the ^{11}B -NMR spectrum). IR (thin film): 2468.2 , 2279.6 , 2210.2 cm^{-1} ν_{BH} . Elemental analysis: found C 33.10, H 7.22; calculated for $[\text{U}(\eta^4\text{-Cb}''')(\mu\text{-BH}_4)_3\{\text{K}(\text{THF})_2\}]_2$ C 32.70, H 7.68.

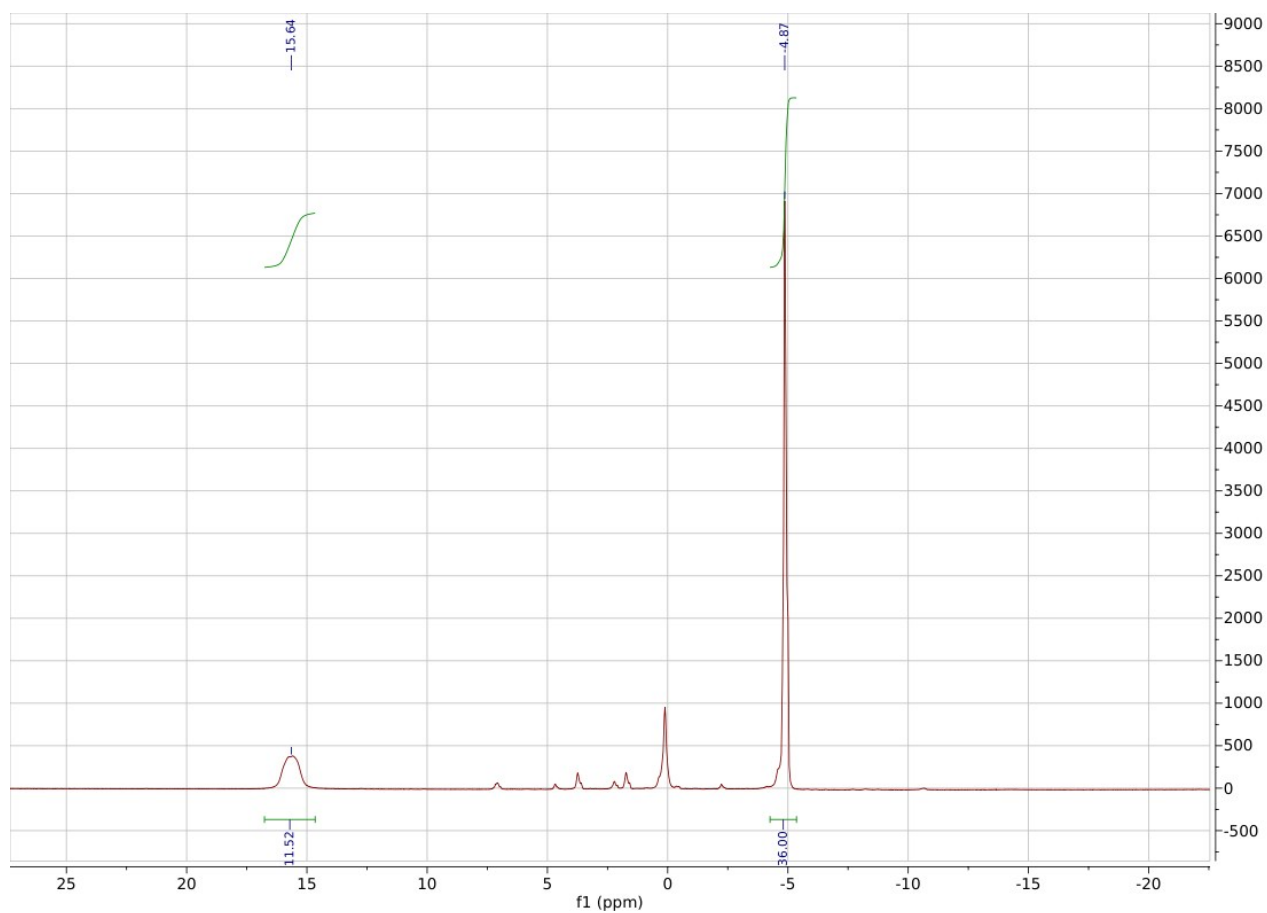


Figure S11. ¹H NMR spectrum of [U(η⁴-Cb''''')(μ-BH₄)₃{K(THF)₂}₂] in THF-D₈.

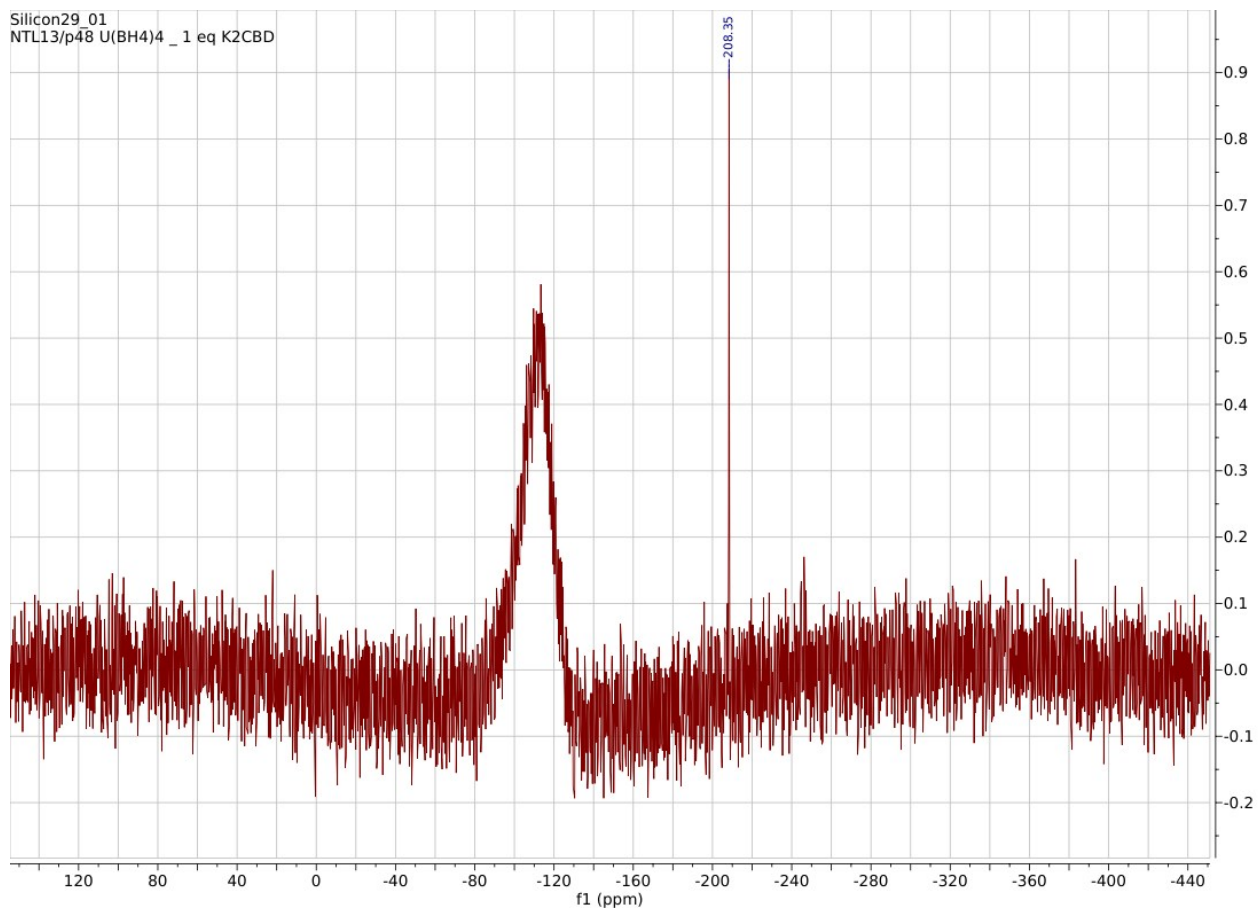


Figure S12. $^{29}\text{Si}\{^1\text{H}\}$ NMR spectrum of $[\text{U}(\eta^4\text{-Cb'''})(\mu\text{-BH}_4)_3\{\text{K}(\text{THF})_2\}_2]$ in THF-D_8 .

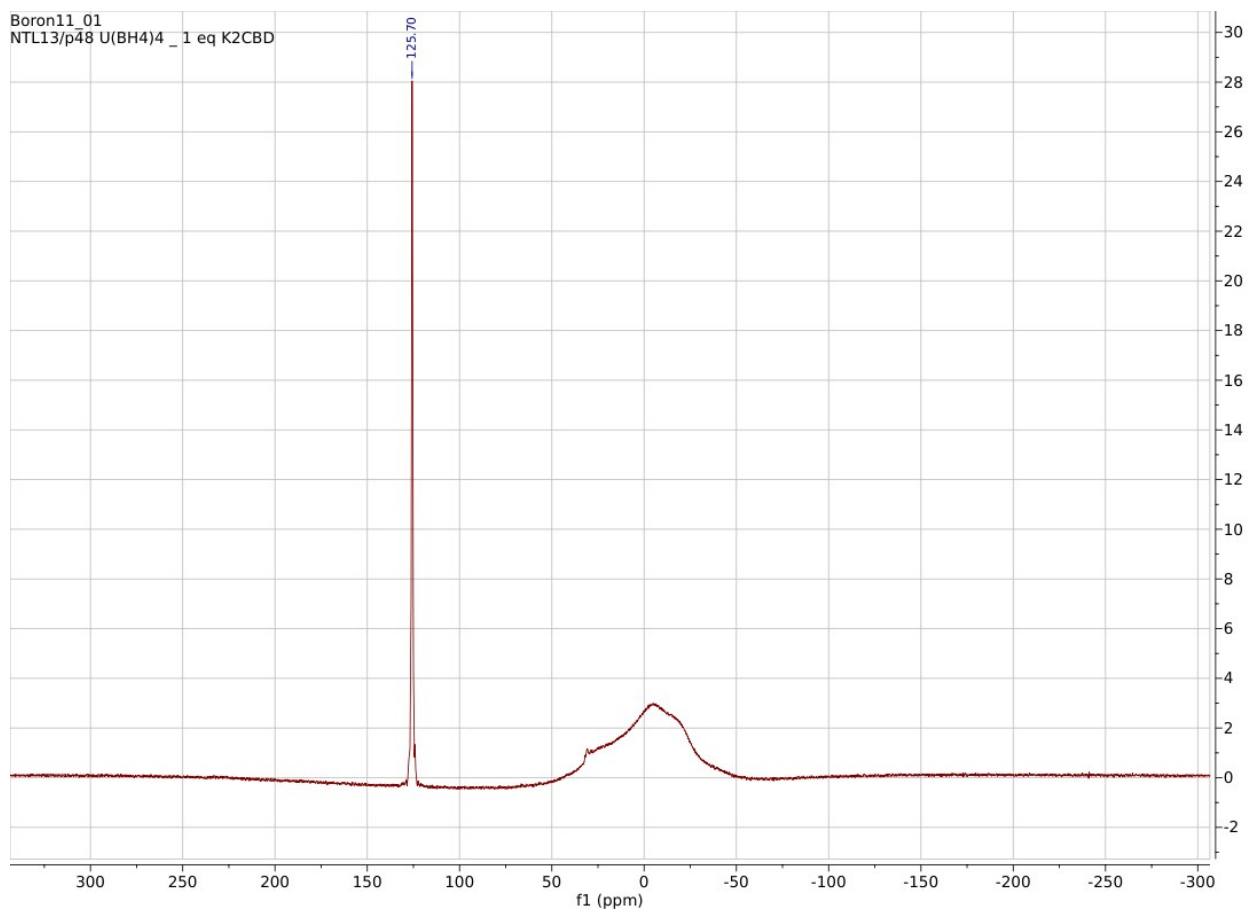


Figure S13. $^{11}\text{B}\{^1\text{H}\}$ NMR spectrum of $[\text{U}(\eta^4\text{-Cb'''})(\mu\text{-BH}_4)_3\{\text{K}(\text{THF})_2\}_2]$ in THF-D_8 .

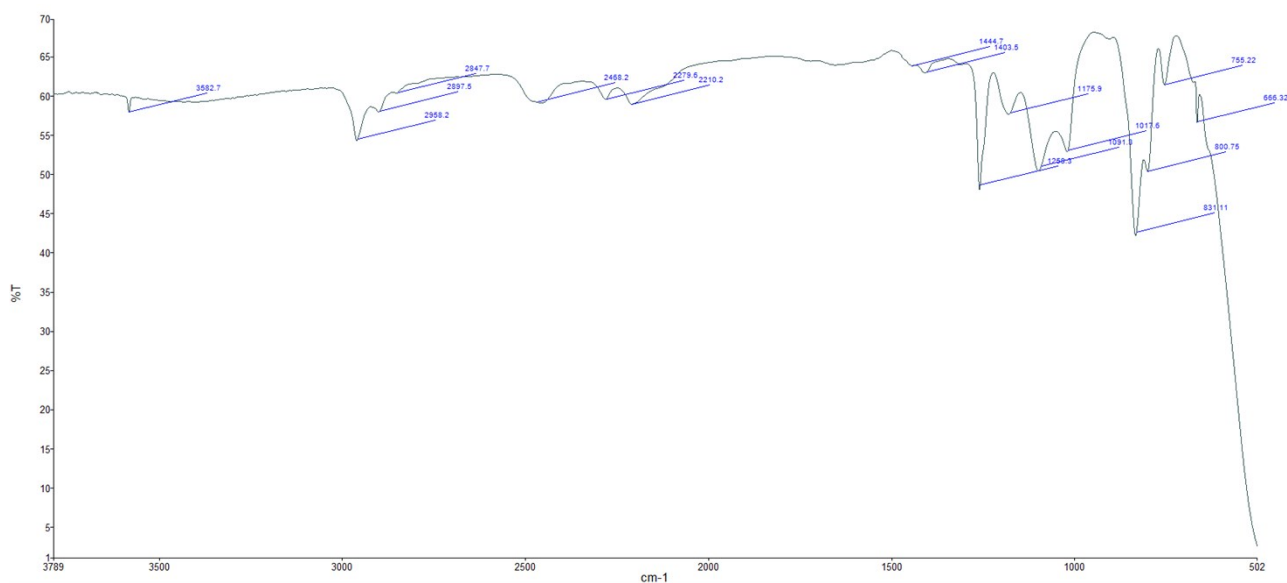
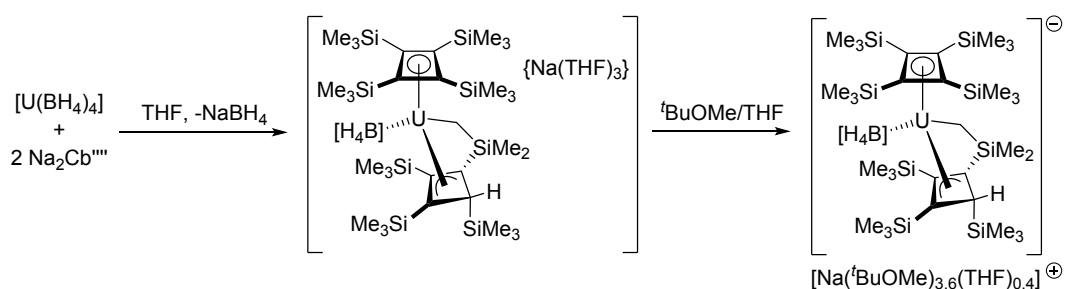


Figure S14. IR spectrum of $[\text{U}(\eta^4\text{-Cb'''})(\mu\text{-BH}_4)_3\{\text{K}(\text{THF})_2\}_2]_2$.

Synthesis of $[\text{U}(\eta^4\text{-Cb}''''')(\eta^3\text{-L}^1)(\mu\text{-BH}_4)\text{Na}(\text{THF})_3]$ and $[\text{U}(\eta^4\text{-Cb}''''')(\eta^3\text{-L}^1)(\mu\text{-BH}_4)][\text{Na}(\text{}^t\text{BuOMe})_{3.6}(\text{THF})_{0.4}]$



A Young's NMR tube was charged with $\text{U}(\text{BH}_4)_4$ (22 mg, 0.074 mmol) and C_7D_8 (*ca* 0.1-0.2 ml) followed by a few drops of THF- D_8 to produce a pale green solution. To this was added a solution of $\text{Na}_2\text{Cb}''''(0.75.\text{THF})$ (65 mg, 0.15 mmol) in THF- D_8 (0.4 ml) resulting in the formation of a brown-red solution, which, after a few minutes, was found by ^1H NMR spectroscopy to consist of $[\text{U}(\eta^4\text{-Cb}''''')(\text{BH}_4)_3][\text{Na}(\text{THF})_n]$ and unreacted $\text{Na}_2\text{Cb}''''(0.75.\text{THF})$ (Figure S15). The reaction was heated overnight at 55°C , followed by spinning for one day at RT and then for another 3 hours at 55°C . The reaction was followed by ^1H NMR spectroscopy until the starting materials were consumed. The reaction mixture was filtered and worked up in the same manner as described for $[\text{U}(\eta^4\text{-Cb}''''')(\text{BH}_4)_3\text{Na}(\text{THF})_3]$, resulting in a brown microcrystalline solid containing *ca* 10% NaBH_4 , as evidenced by $^{11}\text{B}\{^1\text{H}\}$ NMR spectroscopy (Figure S16). The supernatant of this material was filtered and allowed to slowly evaporate to a volume of *ca* 0.5 ml, yielding a second crop of a microcrystalline material (25 mg) subsequently identified by NMR spectroscopy and elemental analysis to be $[\text{U}(\eta^4\text{-Cb}''''')(\eta^3\text{-L}^1)(\mu\text{-BH}_4)\text{Na}(\text{THF})_3]$.

NMR spectra were recorded in THF- D_8 . ^1H NMR (δ/ppm): -148.88 (s, 1H), -106.66 (s, 1H), -82.07 (s, 1H), -78.60 (1:1:1:1 q, $^1J_{\text{BH}} = 66.84$ Hz, 4H, BH_4), -22.18 (s, 3H, SiMe_3), -5.94 (s, 9H, SiMe_3), -0.56 (s, 36H, SiMe_3), 4.37 (s, 9H, SiMe_3), 10.01 (s, 3H, SiMe_3), 12.66 (s, 9H, SiMe_3); $^{29}\text{Si}\{^1\text{H}\}$ NMR: -260.36 , -175.31 , -115 , 56.69 , 66.15 (SiMe_3); $^{23}\text{Na}\{^1\text{H}\}$ NMR: -2.77 (s, $\Delta\nu_{1/2} = 81.67$ Hz); $^{11}\text{B}\{^1\text{H}\}$ NMR: 41.63 (br. s, $\Delta\nu_{1/2} = 225.4$ Hz). Elemental analysis: Found C 45.43, H 8.26; Calculated for $[\text{U}(\eta^4\text{-Cb}''''')(\eta^3\text{-L}^1)(\mu\text{-BH}_4)\text{Na}(\text{THF})_3]$ ($\text{C}_{44}\text{H}_{100}\text{BNaO}_3\text{Si}_8\text{U}$) C 45.02, H 8.59.

Crystals suitable for X-ray diffraction were obtained by dissolving $[\text{U}(\eta^4\text{-Cb}''''')(\eta^3\text{-L}^1)(\mu\text{-BH}_4)\text{Na}(\text{THF})_3]$ (25 mg, 0.021 mmol) in ${}^t\text{BuOMe}$ (*ca* 1.5 ml) containing a few drops of THF. The crystals obtained after *ca* 10 days at -35°C , were subsequently identified by single-crystal X-ray diffraction measurements to be $[\text{U}(\eta^4\text{-Cb}''''')(\eta^3\text{-L}^1)(\mu\text{-BH}_4)][\text{Na}(\text{}^t\text{BuOMe})_{3.6}(\text{THF})_{0.4}]$ (Yield: 8.5 mg, 30%). The ^1H NMR spectrum of this compound in THF- D_8 is virtually identical to $[\text{U}(\eta^4\text{-Cb}''''')(\eta^3\text{-L}^1)(\mu\text{-BH}_4)\text{Na}(\text{THF})_3]$, in addition to featuring two singlets at 1.13 and 3.32 ppm assigned to ${}^t\text{BuOMe}$. The $^{23}\text{Na}\{^1\text{H}\}$ -NMR spectrum shows a small upfield shift to 3.41 ppm ($\Delta\nu_{1/2} = 96.83$ Hz). The $^{11}\text{B}\{^1\text{H}\}$ and $^{29}\text{Si}\{^1\text{H}\}$ NMR spectra are virtually identical. Elemental analysis: Found C 47.00, H 9.19; Calculated for $[\text{U}(\eta^4\text{-Cb}''''')(\eta^3\text{-L}^1)(\mu\text{-BH}_4)][\text{Na}(\text{}^t\text{BuOMe})_{3.6}(\text{THF})_{0.4}]$ ($\text{C}_{52}\text{H}_{124}\text{BNaO}_4\text{Si}_8\text{U}$) C 47.67, H 9.54.

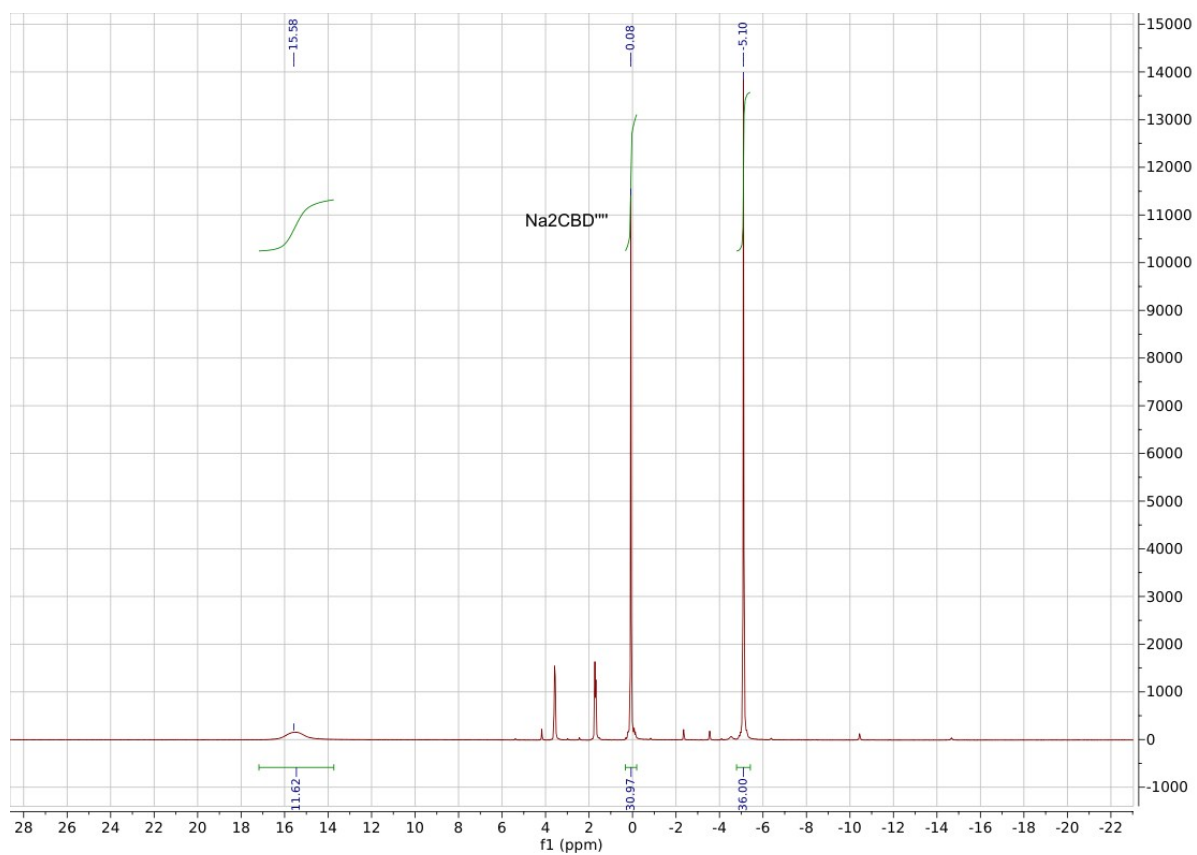


Figure S15. $^1\text{H-NMR}$ spectrum (THF-D_8) of the 2:1 reaction of $\text{Na}_2\text{Cb}(0.75\text{THF})$ with $\text{U}(\text{BH}_4)_4$ shortly after mixing.

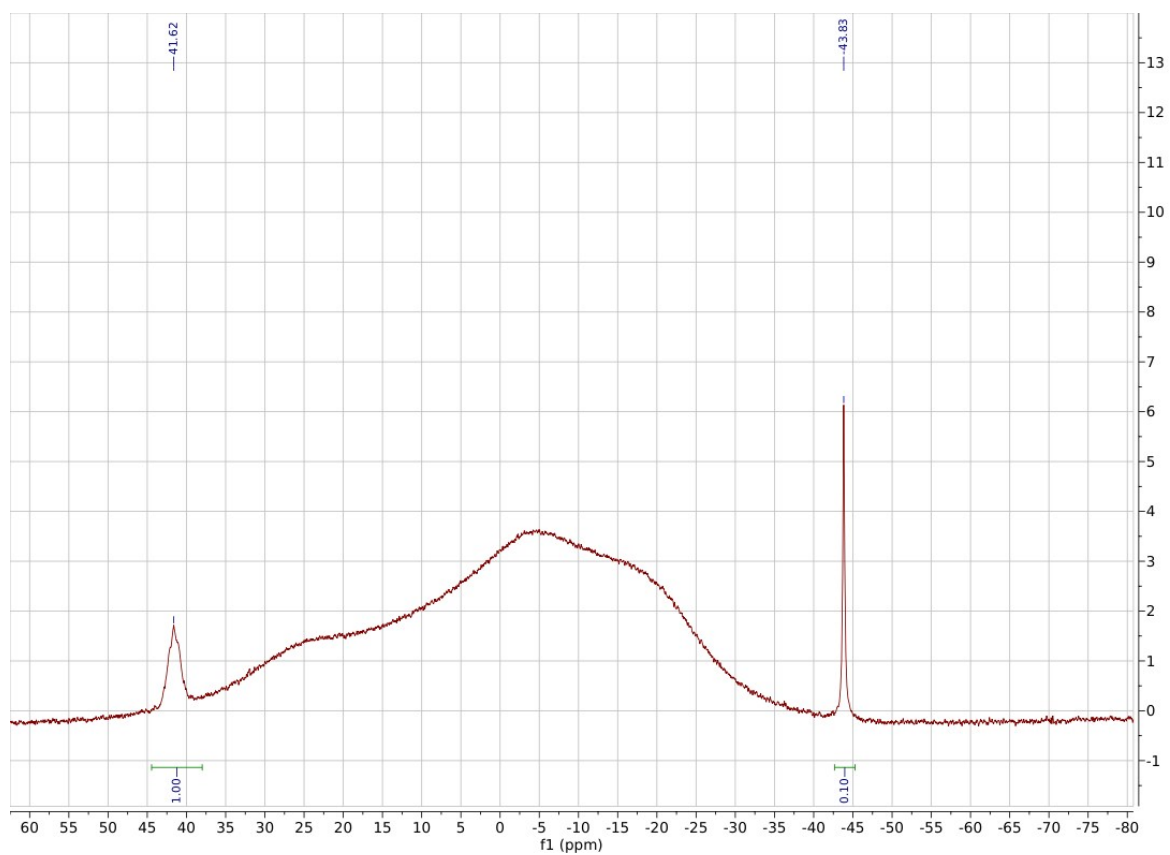


Figure S16. $^{11}\text{B}\{^1\text{H}\}$ NMR spectrum in THF-D_8 of $[\text{U}(\eta^4\text{-Cb}^{\text{III}})(\eta^3\text{-L}^1)(\mu\text{-BH}_4)\text{Na}(\text{THF})_n]$ (41.62 ppm) contaminated with *ca* 10% NaBH_4 (-43.83 ppm).

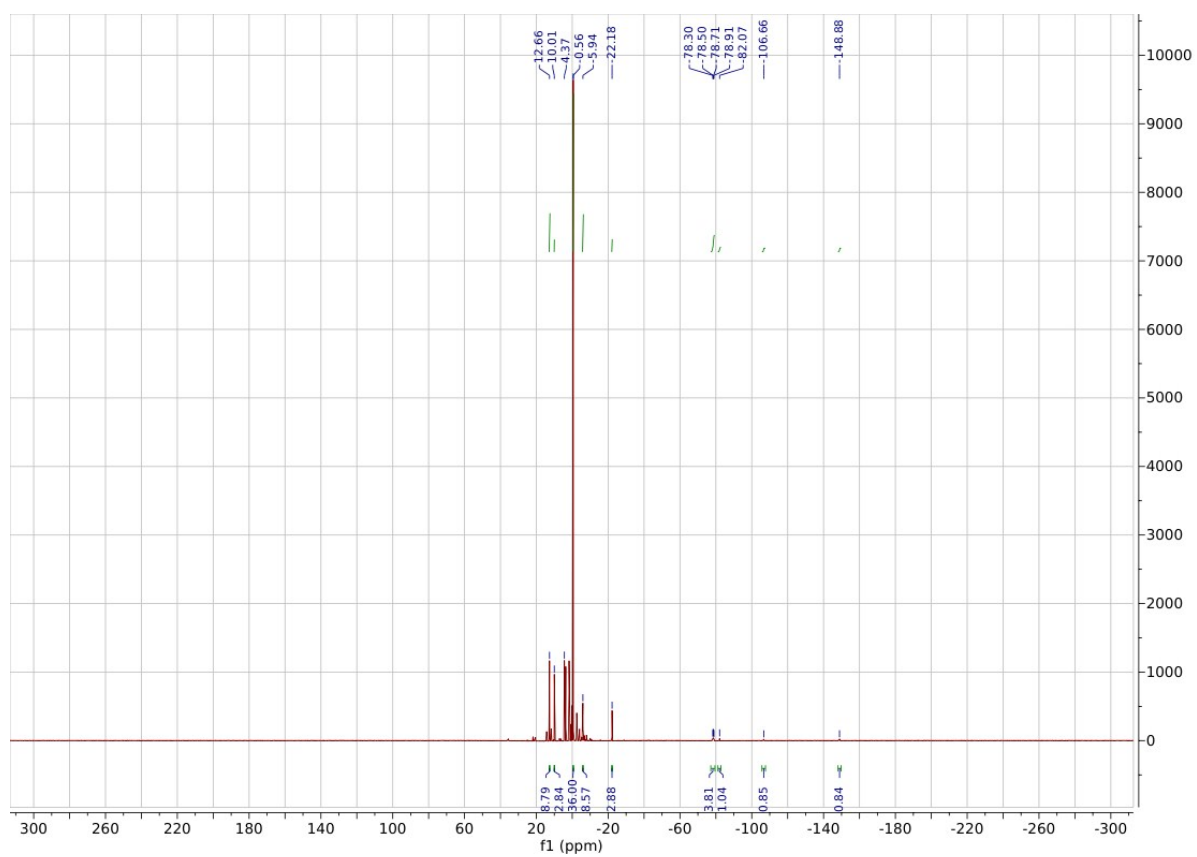


Figure S17. ^1H NMR spectrum of $[\text{U}(\eta^4\text{-Cb'''})(\eta^3\text{-L}^1)(\mu\text{-BH}_4)\text{Na}(\text{THF})_3]$ in THF-D_8 .

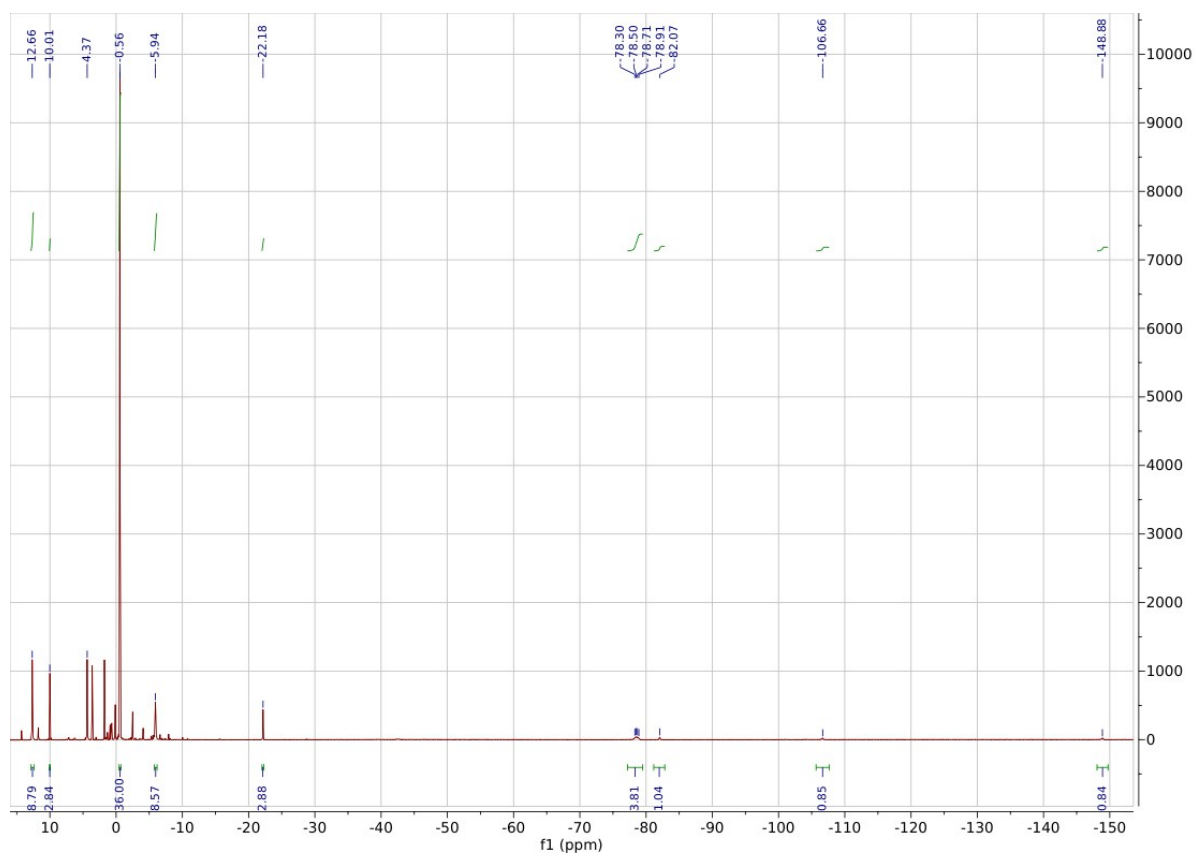


Figure S18. ^1H NMR spectrum of $[\text{U}(\eta^4\text{-Cb''''})(\eta^3\text{-L}^1)(\mu\text{-BH}_4)\text{Na}(\text{THF})_3]$ in THF-D_8 .

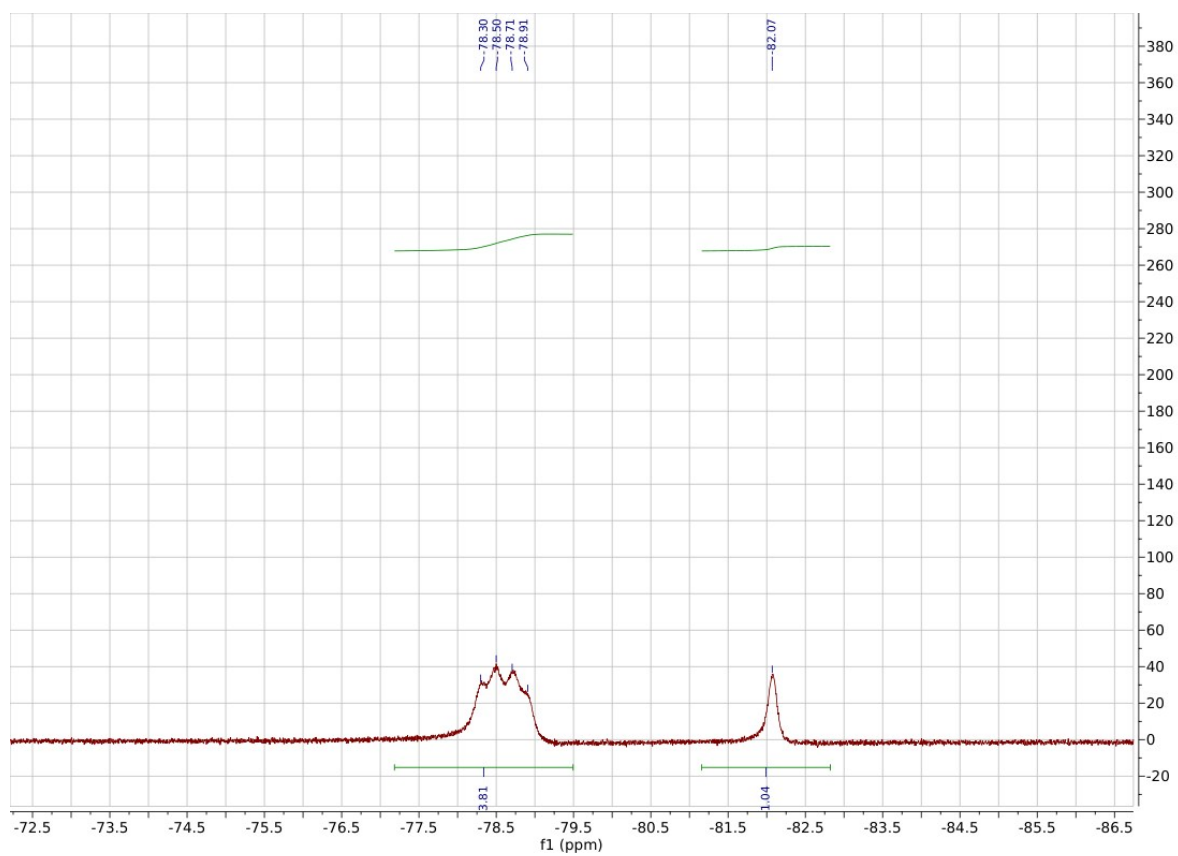


Figure S19. ^1H NMR spectrum of $[\text{U}(\eta^4\text{-Cb}''')(\eta^3\text{-L}^1)(\mu\text{-BH}_4)\text{Na}(\text{THF})_3]$ in THF-D_8 .

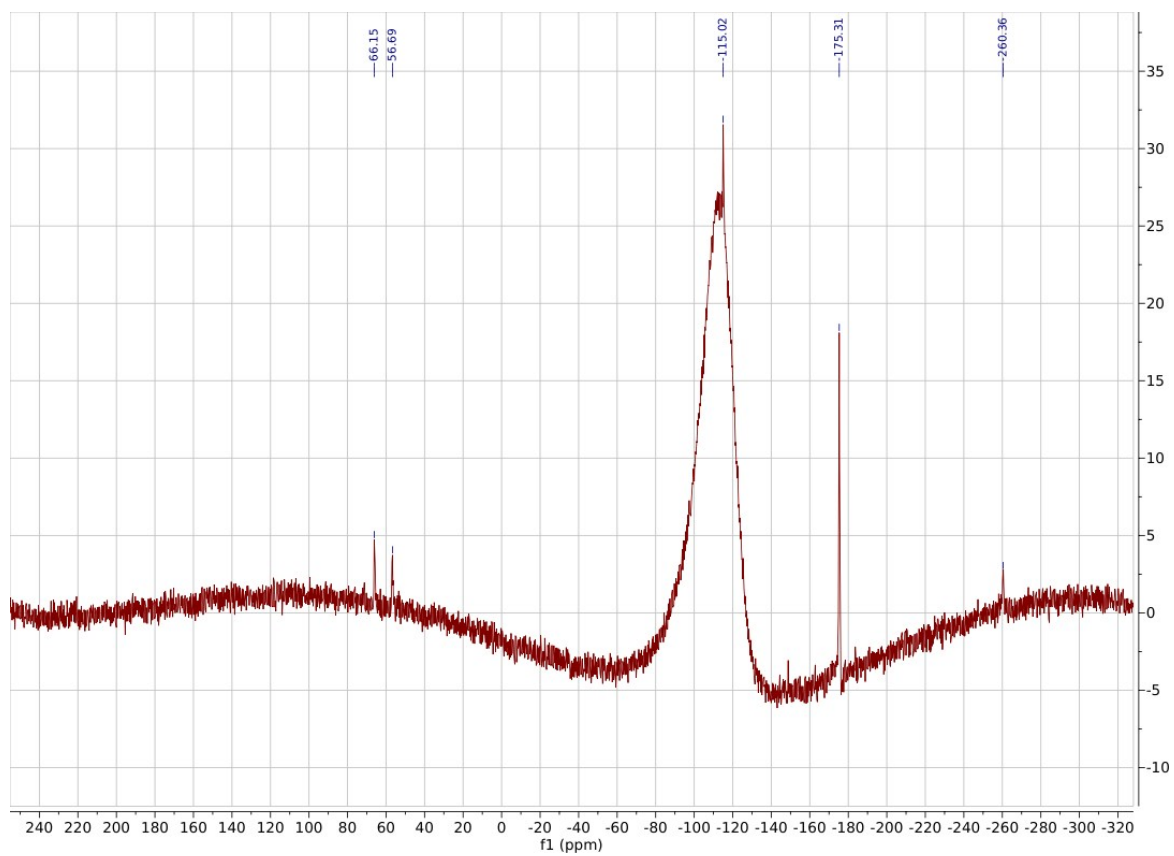


Figure S20. $^{29}\text{Si}\{^1\text{H}\}$ NMR spectrum of $[\text{U}(\eta^4\text{-Cb'''})(\eta^3\text{-L}^1)(\mu\text{-BH}_4)\text{Na}(\text{THF})_3]$ in THF-D_8 .

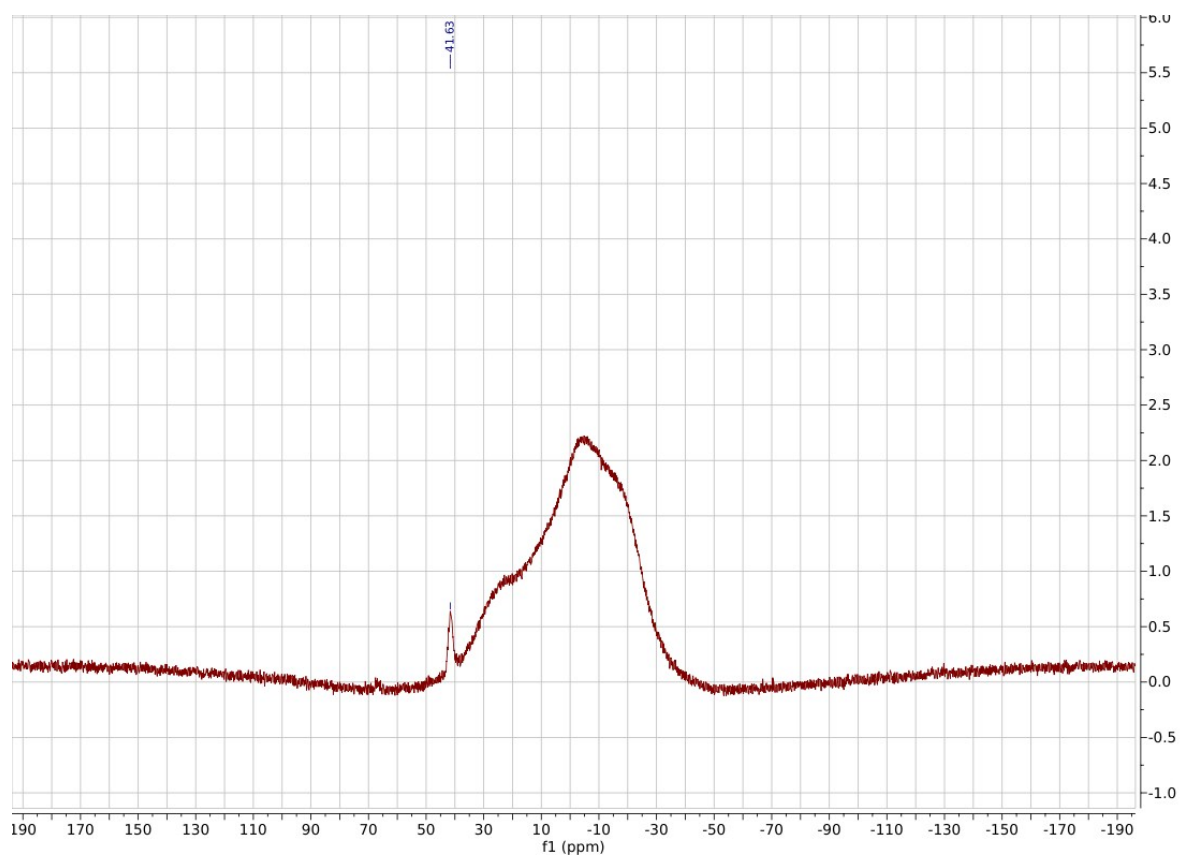


Figure S21. $^{11}\text{B}\{^1\text{H}\}$ NMR spectrum of $[\text{U}(\eta^4\text{-Cb}''')(\eta^3\text{-L}^1)(\mu\text{-BH}_4)\text{Na}(\text{THF})_3]$ in THF-D_8 .

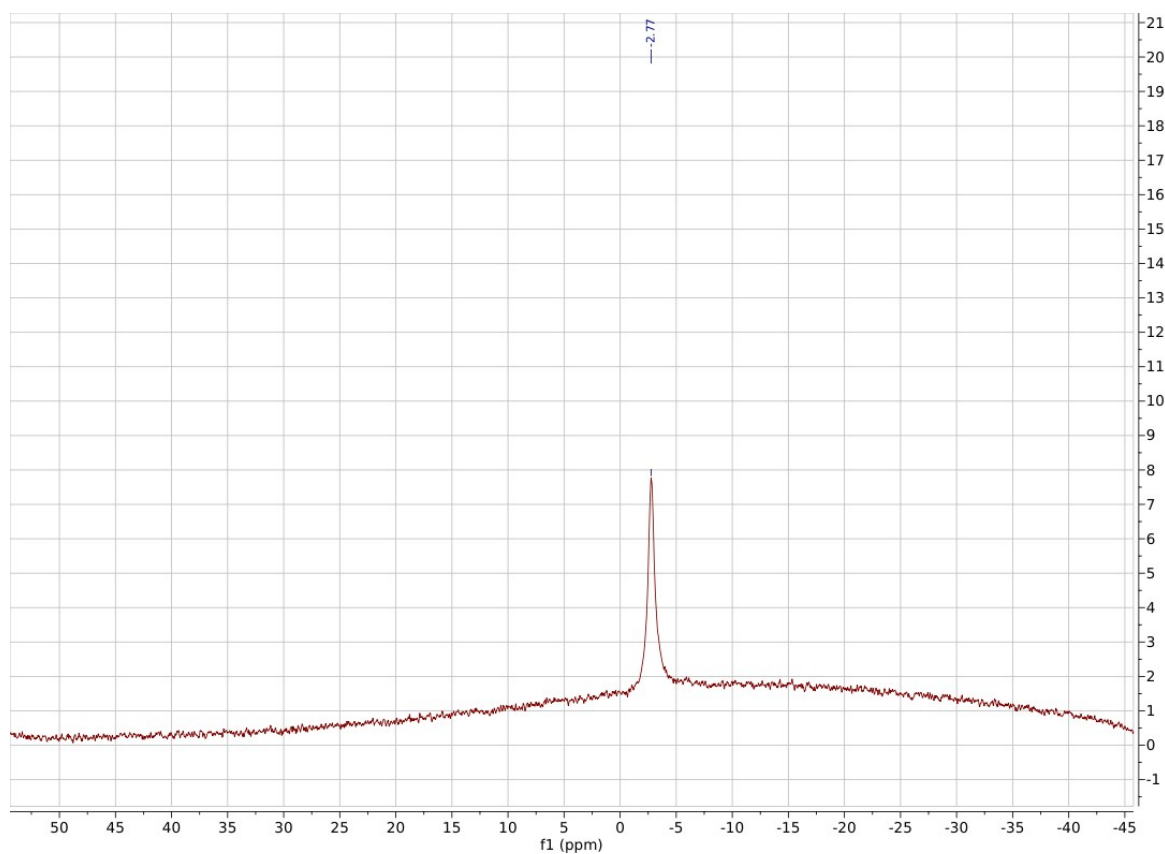


Figure S22. ^{23}Na $\{^1\text{H}\}$ -NMR spectrum of $[\text{U}(\eta^4\text{-Cb'''})(\eta^3\text{-L}^1)(\mu\text{-BH}_4)\text{Na}(\text{THF})_3]$ in THF-D_8 .

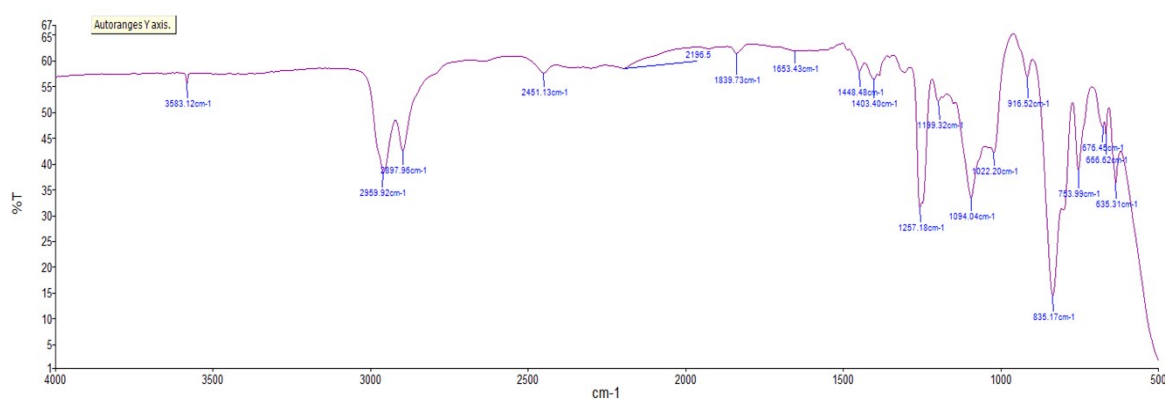


Figure S23. IR spectrum of $[\text{U}(\eta^4\text{-Cb'''})(\eta^3\text{-L}^1)(\mu\text{-BH}_4)\text{Na}(\text{THF})_3]$.

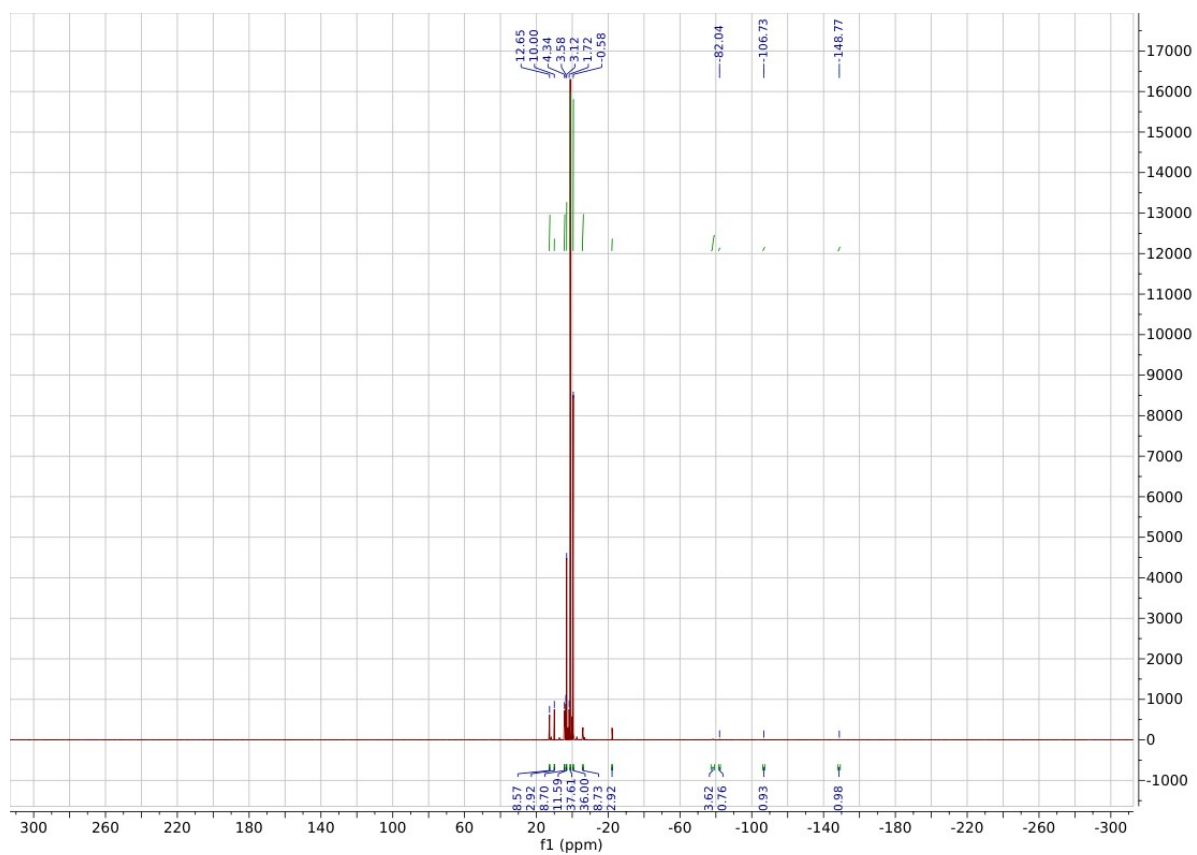


Figure S24. ^1H NMR spectrum of $[\text{U}(\eta^4\text{-Cb}^{\text{III}})(\eta^3\text{-L}^1)(\mu\text{-BH}_4)][\text{Na}(\text{tBuOMe})_{3.6}(\text{THF})_{0.4}]$ in THF-D_8 .

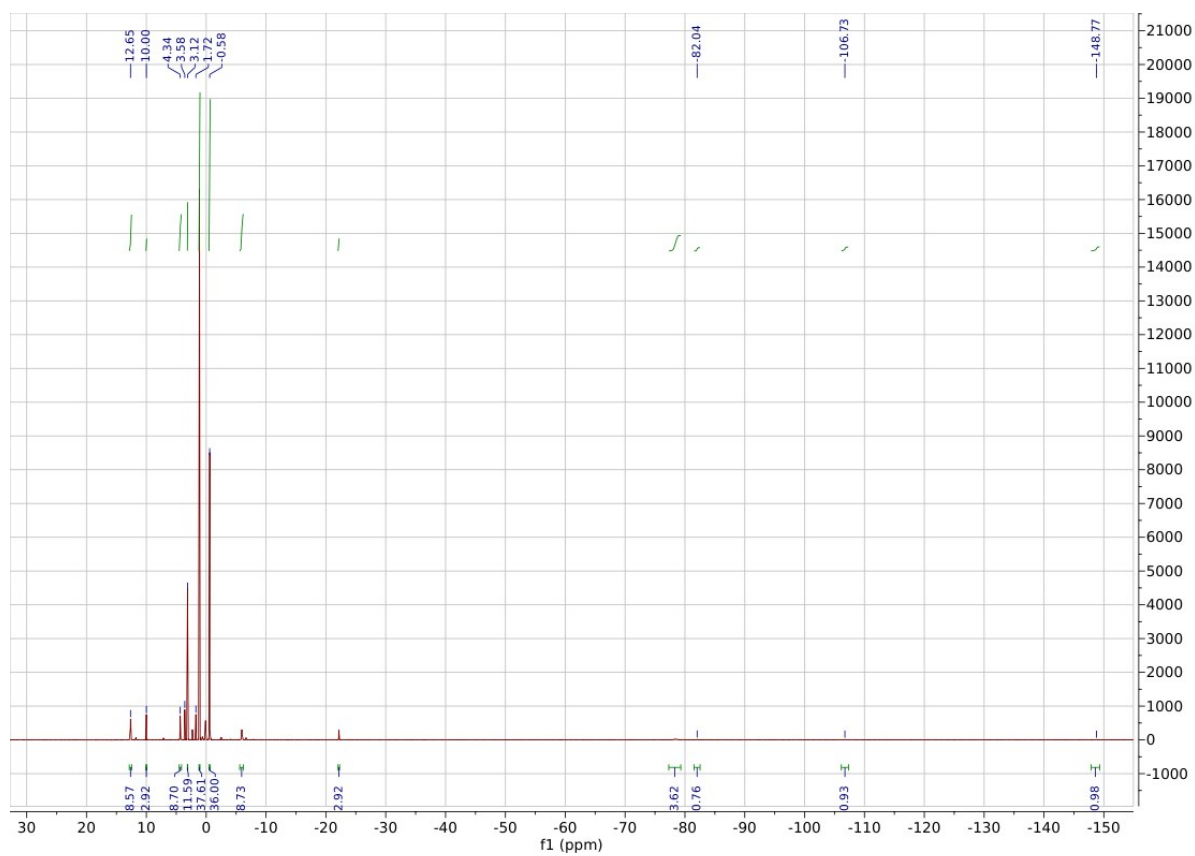


Figure S25. ^1H NMR spectrum of $[\text{U}(\eta^4\text{-Cb''''})(\eta^3\text{-L}^1)(\mu\text{-BH}_4)][\text{Na}(\text{tBuOMe})_{3.6}(\text{THF})_{0.4}]$ in THF-D_8 . Peaks at 1.13 and 3.72 ppm correspond to tBuOMe .

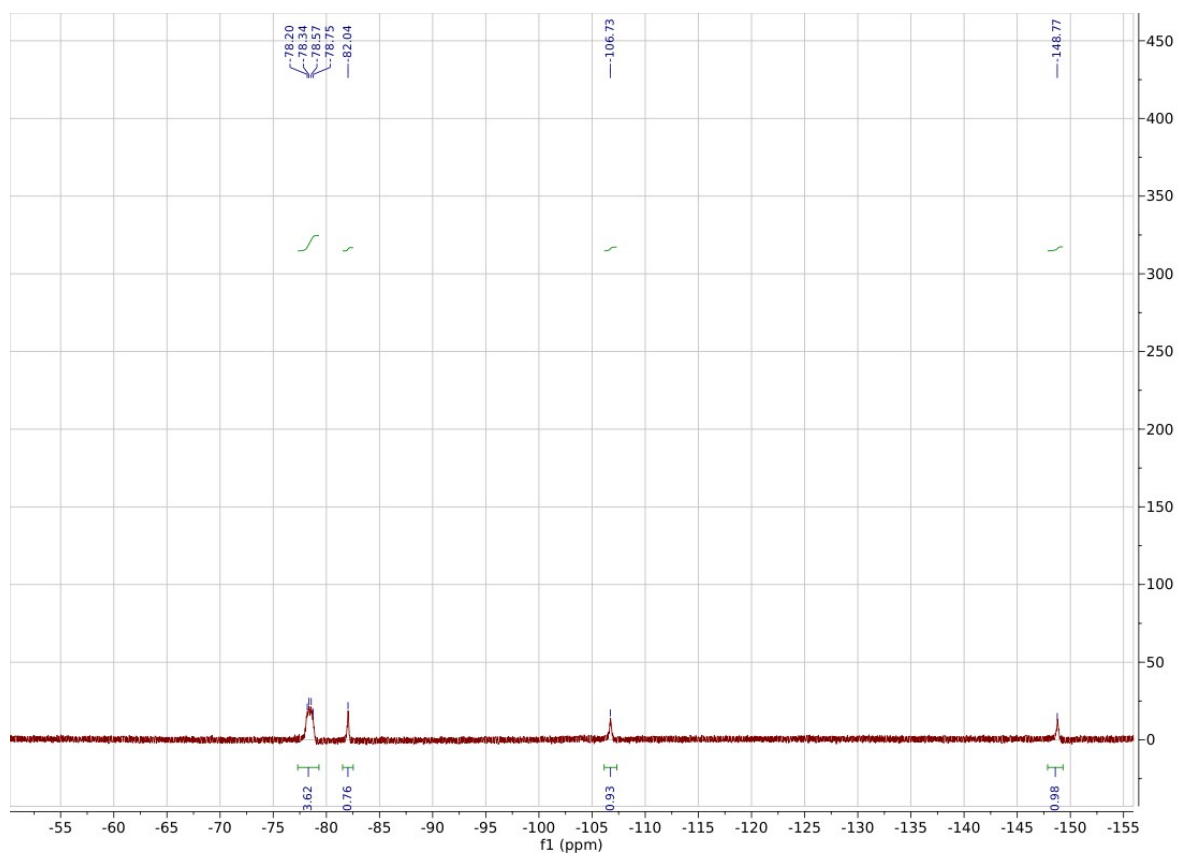


Figure S26. ¹H NMR spectrum in the region -55 and -155 ppm of [U(η⁴-Cb''''(η³-L¹)(μ-BH₄))[Na(^tBuOMe)_{3.6}(THF)_{0.4}] in THF-D₈.

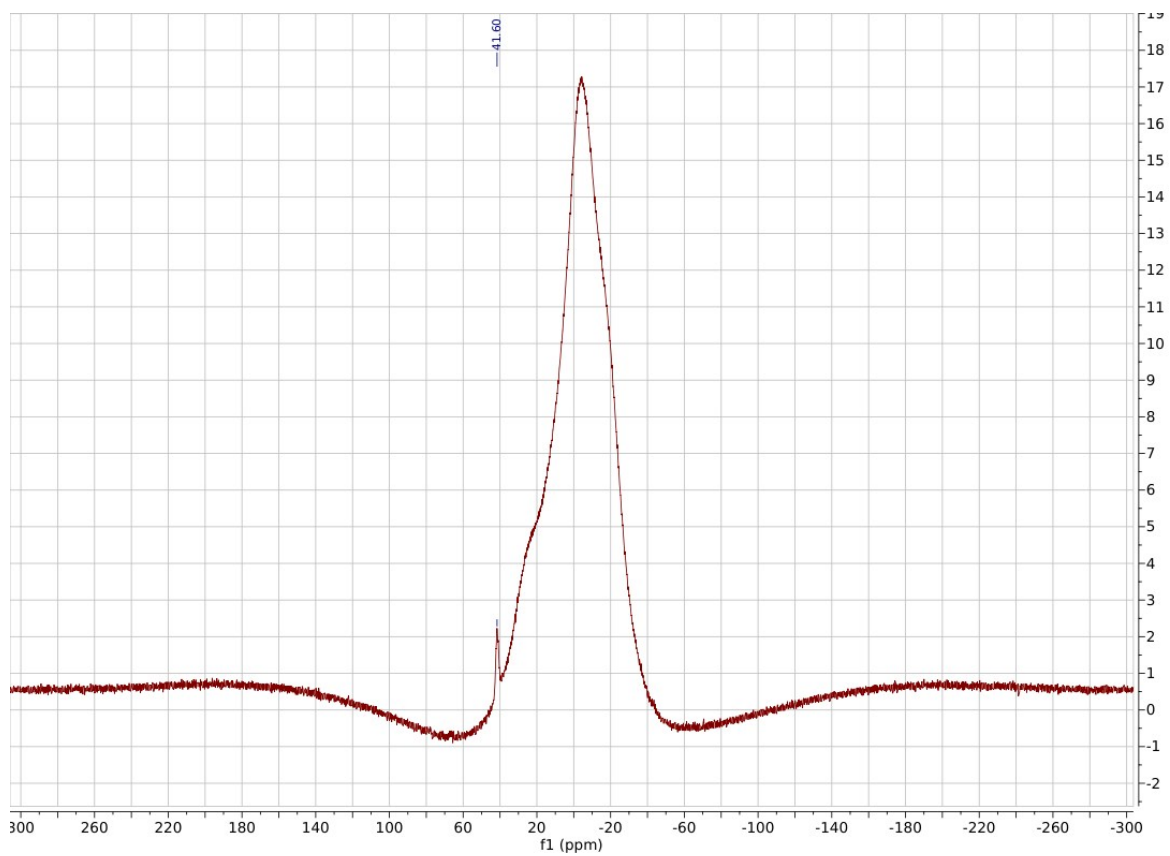


Figure S27. $^{11}\text{B}\{^1\text{H}\}$ NMR spectrum of $[\text{U}(\eta^4\text{-Cb'''})(\eta^3\text{-L}^1)(\mu\text{-BH}_4)][\text{Na}(\text{tBuOMe})_{3.6}(\text{THF})_{0.4}]$ in THF-D_8 .

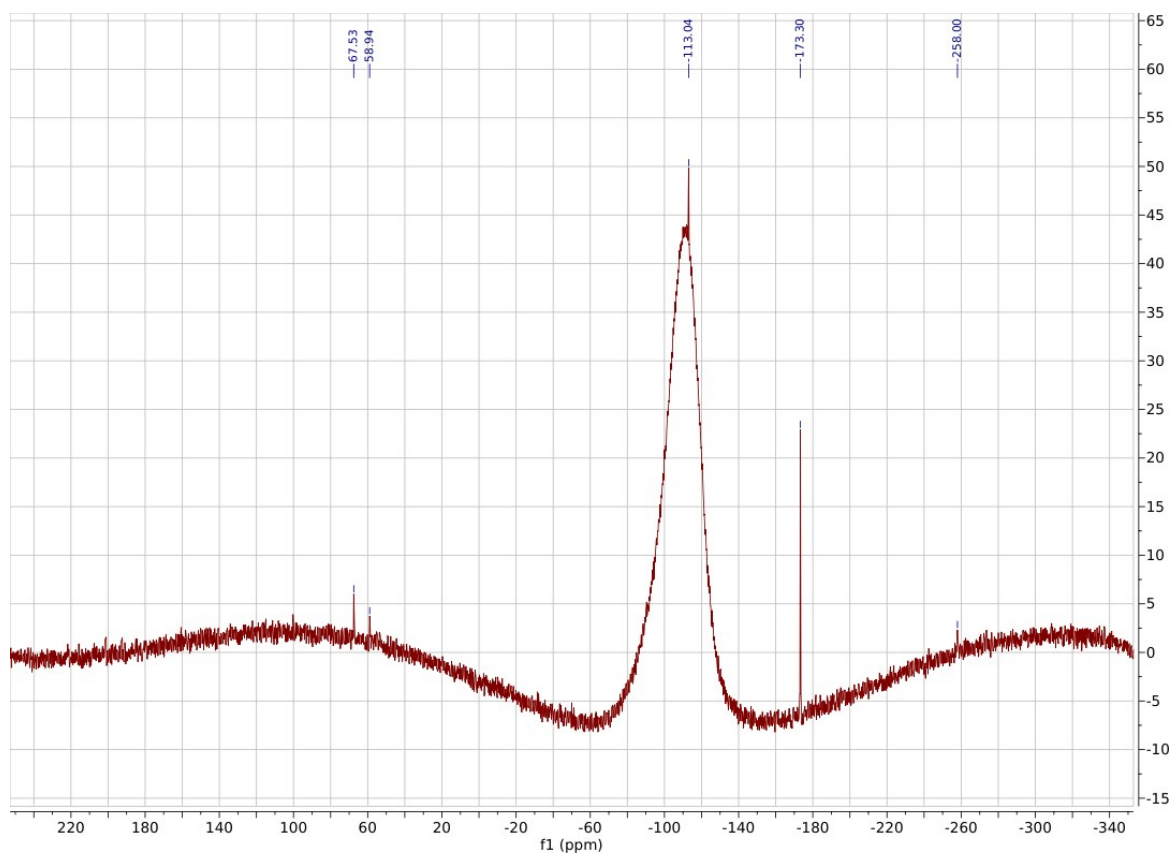


Figure S28. $^{29}\text{Si}\{^1\text{H}\}$ NMR spectrum of $[\text{U}(\eta^4\text{-Cb'''})(\eta^3\text{-L}^1)(\mu\text{-BH}_4)][\text{Na}(\text{tBuOMe})_{3.6}(\text{THF})_{0.4}]$ in THF- D_8 .

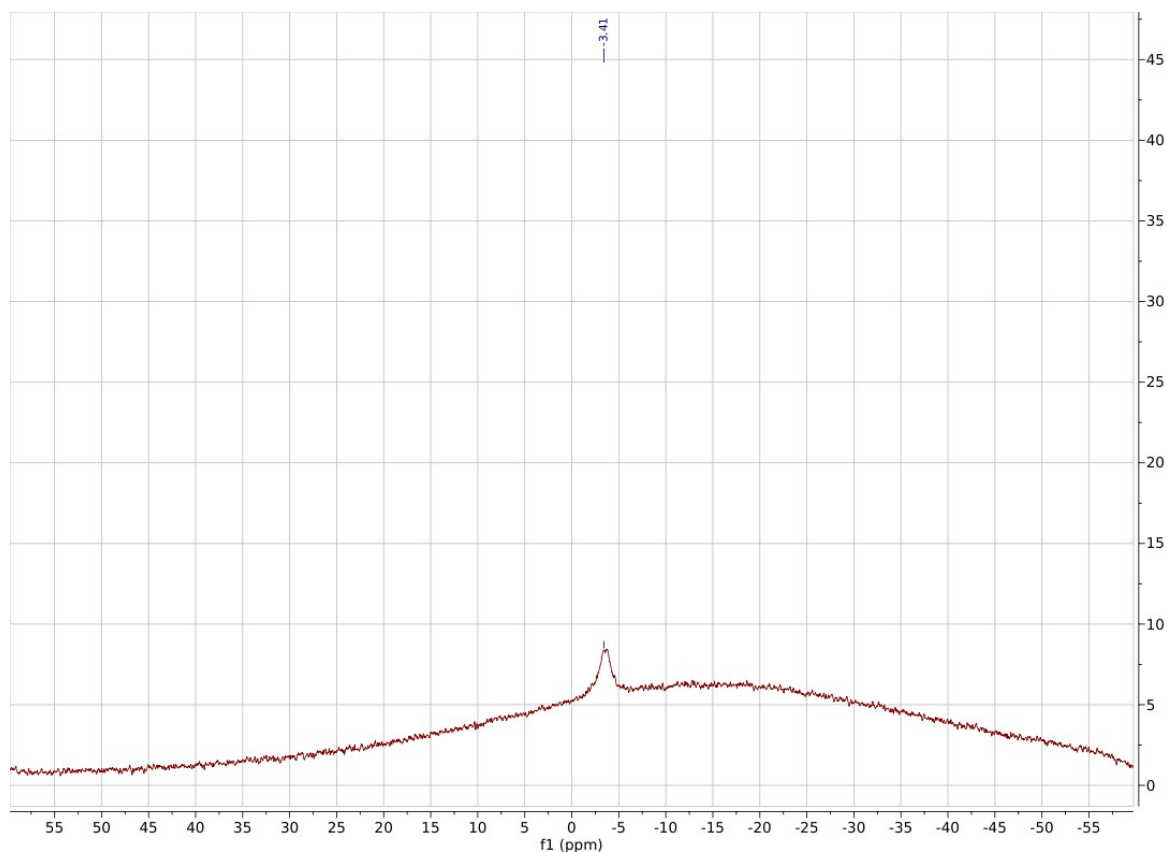


Figure S29. $^{23}\text{Na}\{^1\text{H}\}$ NMR spectrum of $[\text{U}(\eta^4\text{-Cb'''})(\eta^3\text{-L}^1)(\mu\text{-BH}_4)][\text{Na}(\text{tBuOMe})_{3.6}(\text{THF})_{0.4}]$ in THF-D_8 .

X-ray Crystallography

Data for compounds $[\text{Na}(12\text{-c-4})_2][\text{U}(\text{Cb'''})(\text{BH}_4)_3]$ ($[\text{Na}(12\text{-crown-4})_2][\mathbf{1}]$) and $[\text{Na}(\text{tBuOMe})_{3.6}(\text{THF})_{0.4}][\text{U}(\text{Cb'''})(\text{L}^1)(\mu\text{-BH}_4)]$ ($[\text{Na}(\text{tBuOMe})_{3.6}(\text{THF})_{0.4}][\mathbf{3}]$) and were collected using an Agilent Gemini Ultra diffractometer with an Enhance Ultra ($\text{Cu } K\alpha$) sealed tube source, equipped with an Eos CCD area detector, operating in ω scanning mode to fill the Ewald sphere. All data collections were carried out at 100 K. Control, integration and absorption correction were handled by the CrysAlis^{Pro} software. The crystals were mounted on MiTiGen loops, from dried vacuum oil kept over 4 Å in an MBraun glovebox under Ar. All solutions and refinements were performed using the Olex2 package and all software packages within.⁵ All non-hydrogen atoms were refined using anisotropic thermal parameters, and hydrogens were added using a riding model, except in the case of B-H bonds that were found in the difference map and refined freely. In the case of $[\text{U}(\text{Cb'''})(\mu\text{-BH}_4)_3\{\text{K}(\text{THF})_2\}]_2$ ($\mathbf{2}$) data were collected on a Rigaku FR-E rotating $\text{Cu } K\alpha$ anode at 100 K equipped with a HyPix area detector at the National Crystallography Service at the University of Southampton.⁶ The crystal was found to be a non-merohedral twin and this was handled by the twinning facility within the CrysAlis^{Pro} software. Due to the quality of the crystals, we could not locate the B-H hydrogen atoms in the difference map and therefore they are not included in the model. In the case of $[\text{Na}(12\text{-c-4})_2][\mathbf{1}]$ solvent accessible voids were found using Platon which correspond to the dioxane crystallisation solvent (no electron density peaks could be located though). The B-alert associated with the BH distance is erroneous as the hydrogen atoms have been properly placed in their positions according to the electron density difference map. In the case of compound $\mathbf{2}$, a B-alert arises from disorder of a THF molecule coordinated to potassium. A second B-alert arises due to weak diffraction in some of the high-resolution frames (but very close to the I/σ cut-off point), since the crystal is twin. In the case of $[\text{Na}(\text{tBuOMe})_{3.6}(\text{THF})_{0.4}][\mathbf{3}]$, extensive disorder was present around the Na^+ cation causing some an A-alert; this disorder was treated by the use of RIGU, DFIX, DANG, SIMU, DELU and EADP restraints/constraints, where applicable; some of the ellipsoids are still abnormal, thus giving rise to Level C alerts.

Table S1. Crystal data and structure refinement for [Na(12-crown-4)₂][1], **2** and [Na(^tBuOMe)_{3.6}(THF)_{0.4}][3].

Compound	[Na(12-crown-4) ₂][1]	2	[Na(^t BuOMe) _{3.6} (THF) _{0.4}][3]
CCDC ref. code	1966628	1966629	1966630
Colour, Habit	Light Bronze, Plate	Brown, Plate	Dark Brown, Block
Size/mm	0.01 × 0.15 × 0.2	0.01 × 0.1 × 0.1	0.08 × 0.1 × 0.15
Empirical Formula	C ₃₂ H ₇₉ B ₃ NaO ₈ Si ₄ U	C ₂₄ H ₆₄ B ₃ KO ₂ U	C ₅₂ H _{123.7} BNaO ₄ Si ₈ U
M	997.76	794.57	1309.75
Crystal System	Monoclinic	Monoclinic	Monoclinic
Space Group	<i>P</i> 2 ₁ / <i>n</i>	<i>P</i> 2 ₁ / <i>c</i>	<i>P</i> 2 ₁ / <i>c</i>
<i>a</i> /Å	17.3922(2)	15.5143(5)	13.20381(14)
<i>b</i> /Å	14.5028(2)	15.8092(8)	26.1179(3)
<i>c</i> /Å	20.3353(2)	16.0534(5)	20.8685(2)
α°	90	90	90
β°	108.8680(10)	97.572(3)	97.5838(11)
γ°	90	90	90
V/ Å ³	4853.67(10)	3903.1(13)	7133.65(14)
Z	4	4	4
μ /mm ⁻¹	10.755	13.959	8.013
T (K)	100	100	100
θ min/max	3.817/71.197	2.873/68.359	3.377/67.070
Completeness	98.7 to 71.197	99.8 to 68.359	99.4 to 67.070
Reflections Total/Independent	9293/8285	14621/7876	12686/10641
<i>R</i> _{int}	0.0377	0.1552	0.0333
Final <i>R</i> 1 and <i>wR</i> 2	0.0359/0.0960	0.0991/0.3009	0.0437/0.1123
Goof	1.026	0.976	1.042
Largest peak hole/ e.Å ⁻³	2.0 and -1.0	3.6 and -1.1	3.4 and -2.5
ρ_{calc} /g.cm ⁻³	1.365	1.352	1.220

Computational Details

The calculations carried out at density functional theory (DFT) level of theory using the Amsterdam Density Functional (ADF2019) code.⁷⁻⁹ The geometries were extracted from the crystal structures. Positions of hydrogen atoms were optimized using the pure PBE exchange-correlation (XC) functional^{10,11} while the positions of heavier atoms were kept frozen to their crystal-structure coordinates. The counter ions were excluded from the calculations. The ground state spin state was confirmed as a triplet both for **1** and **2** and this was used in all subsequent calculations. The bonding analyses were based on single-point energy calculations using the PBE0 hybrid XC functional^{12,13} and the geometries with optimized hydrogen positions. The reported orbital contributions are based on decomposition of the molecular orbitals into non-orthogonal fragment orbitals. The fragment orbitals are the results of a variational calculation on the fragments except in the case of the U(IV) ion, which was calculated using restricted orbitals due to limitation of the ADF code on the nature of the fragment orbitals.

The zeroth order regular approximation (ZORA)¹⁴⁻¹⁶ was used throughout to account for scalar relativistic effects. Slater-type (STO) all-electron basis sets specifically design for scalar relativistic calculations were used in all calculations¹⁷. Triple- ζ quality basis sets with two sets of polarization functions (TZ2P) were used for uranium, for the B, C and H atoms on the Cb rings, on the coordinated CH₂ group, and the BH₄⁻ anions. A triple- ζ basis with one set of polarization functions (TZP) was used for the Si atoms and a polarized double- ζ basis was used for other atoms. The “NumericalQuality” keyword in ADF was set to “Good” to reduce numerical noise in the SCF.

Table S2. Decomposition of the valence molecular orbitals of **1** into fragment orbitals. The numbers quoted are percentages and the numbers in the top row are the orbital indices.

	152	153	154	155	152	153
$7s$	3.37	0.00	0.14	0.02	0.01	0.00
$6d_{xy}$	0.44	0.00	8.04	2.18	9.15	0.12
$6d_{yz}$	0.03	0.04	1.66	8.99	0.08	9.08
$5f_{z^3}$	26.61	0.00	2.13	2.21	0.03	1.98
$5f_{z(x^2-y^2)}$	26.39	1.19	0.01	4.95	0.09	3.64
$5f_{xyz}$	1.14	31.81	1.01	1.62	0.36	0.04
$5f_{xz^2}$	0.97	1.98	0.05	0.17	0.00	0.00
$5f_{yz^2}$	13.49	33.73	3.63	2.13	0.01	0.01
$5f_{x(x^2-3y^2)}$	3.02	4.10	3.56	0.43	4.43	0.07
$5f_{y(3x^2-y^2)}$	17.31	15.35	2.42	0.32	0.43	0.09
Cb HOMO	2.76	0.78	60.38	0.87	67.35	3.12
Cb HOMO	0.03	1.75	1.29	60.94	3.05	66.84

Table S3. Decomposition of the valence molecular orbitals of **2** into fragment orbitals. The numbers quoted are percentages and the numbers in the top row are the orbital indices.

	235	236	237	238	239	240	235	236	237	238
$7s$	1.14	0.2	0.05	1.47	0.01	0.04	0.91	0.41	0.04	0.01
$8s$	0.14	0.00	0.01	-0.04	0.00	0.01	0.17	-0.05	0.00	0.00
$6d_{x^2}$	1.99	0.40	0.17	0.13	2.96	0.77	1.99	0.08	2.77	0.13
$6d_{x^2-y^2}$	7.77	2.78	0.35	0.00	0.25	0.10	8.35	1.39	0.42	0.19
$6d_{xy}$	3.20	7.28	0.96	1.08	0.16	2.8	1.63	9.24	0.23	2.05
$6d_{xz}$	0.00	0.00	0.04	0.07	4.73	1.00	0.00	0.00	4.26	0.44
$6d_{yz}$	1.72	0.11	0.17	0.05	0.05	2.14	1.68	0.01	0.04	1.86
$5f_{z^3}$	0.42	5.75	0.36	52.12	0.11	4.20	0.09	0.01	0.00	0.06
$5f_{z(x^2-y^2)}$	0.00	3.19	12.03	9.26	0.06	3.32	0.10	0.01	1.11	0.06
$5f_{xyz}$	1.25	5.77	21.75	0.99	3.22	0.46	0.16	1.10	0.01	0.31
$5f_{xz^2}$	0.02	0.22	6.95	1.52	2.00	0.76	0.01	0.07	3.04	0.20
$5f_{yz^2}$	0.76	0.02	24.87	1.90	2.91	0.40	0.20	0.06	0.04	0.52
$5f_{x(x^2-3y^2)}$	0.04	0.60	19.28	5.62	3.28	1.94	0.05	0.39	0.33	0.6
$5f_{y(3x^2-y^2)}$	5.11	0.00	0.02	1.71	1.46	3.00	3.4	0.35	0.56	2.98
Cb' HOMO	0.36	9.01	0.78	0.04	23.2	35.49	0.05	8.80	18.68	45.88
Cb' HOMO	0.00	2.37	4.83	1.40	36.44	20.96	0.04	1.20	51.94	18.33
Cb HOMO	0.73	47.88	1.60	15.36	2.69	11.68	2.95	61.71	0.61	16.78
Cb HOMO	64.47	0.20	0.52	0.36	0.39	0.09	66.81	3.25	0.13	0.25

References

- 1 A. Haaland, D. J. Shorokhov, A. V Tutukin, H. V. Volden, O. Swang, G. S. McGrady, N. Kaltsoyannis, A. J. Downs, C. Y. Tang and J. F. C. Turner, *Inorg. Chem.*, 2002, **41**, 6646–6655.
- 2 B. M. Day, F.-S. Guo, S. R. Giblin, A. Sekiguchi, A. Mansikkamäki and R. A. Layfield, *Chem. - Eur. J.*, 2018, **24**, 16779–16782.
- 3 A. Chakraborty, B. M. Day, J. P. Durrant, M. He, J. Tang and R. A. Layfield, *Organometallics*, 2019, DOI: 10.1021/acs.organomet.9b00763.
- 4 A. Sekiguchi, T. Matsuo and H. Watanabe, *J. Am. Chem. Soc.*, 2000, **122**, 5652–5653.
- 5 O. V Dolomanov, L. J. Bourhis, R. J. Gildea, J. A. K. Howard and H. Puschmann, *J. Appl. Crystallogr.*, 2009, **42**, 339–341.
- 6 S. J. Coles and P. A. Gale, *Chem. Sci.*, 2012, **3**, 683–689.
- 7 ADF 2019.3 SMC, Theoretical Chemistry, Vrije Universiteit, Amsterdam, The Netherlands, <http://www.scm.com>. E. J. Baerends, T. Ziegler, A. J. Atkins, J. Autschbach, D. Bashford, O. Baseggio, A. Bérces, F. M. Bickelhaupt, C. Bo, P. M. Boerritger, L. Cavallo, C. Daul, D. P. Chong, D. V Chulhai, L. Deng, R. M. Dickson, J. M. Dieterich, D. E. Ellis, M. van Faassen, A. Ghysels, A. Giammona, S. J. A. van Gisbergen, A. Goetz, A. W. Götz, S. Gusarov, F. E. Harris, P. van den Hoek, Z. Hu, C. R. Jacob, H. Jacobsen, L. Jensen, L. Joubert, J. W. Kaminski, G. van Kessel, C. König, F. Kootstra, A. Kovalenko, M. Krykunov, E. van Lenthe, D. A. McCormack, A. Michalak, M. Mitoraj, S. M. Morton, J. Neugebauer, V. P. Nicu, L. Noodleman, V. P. Osinga, S. Patchkovskii, M. Pavanello, C. A. Peeples, P. H. T. Philipsen, D. Post, C. C. Pye, H. Ramanantoanina, P. Ramos, W. Ravenek, J. I. Rodríguez, P. Ros, R. Rüger, P. R. T. Schipper, D. Schlüns, H. van Schoot, G. Schreckenbach, J. S. Seldenthuis, M. Seth, J. G. Snijders, M. Solà, S. M., M. Swart, D. Swerhone, G. te Velde, V. Tognetti, P. Vernooijs, L. Versluis, L. Visscher, O. Visser, F. Wang, T. A. Wesolowski, E. M. van Wezenbeek, G. Wiesenekker, S. K. Wolff, T. K. Woo and A. L. Yakovlev, 2019.
- 8 G. te Velde, F. M. Bickelhaupt, E. J. Baerends, C. Fonseca Guerra, S. J. A. van Gisbergen, J. G. Snijders and T. Ziegler, *J. Comp. Chem.*, 2001, **22**, 931–967.
- 9 C. Fonseca Guerra, J. G. Snijders, G. te Velde and E. J. Baerends, *Theor. Chem. Acc.*, 1998, **99**, 391–403.
- 10 J. P. Perdew, K. Burke and M. Ernzerhof, *Phys. Rev. Lett.*, 1996, **77**, 3865–3868.
- 11 J. P. Perdew, K. Burke and M. Ernzerhof, *Phys. Rev. Lett.*, 1997, **78**, 1396.
- 12 C. Adamo and V. Barone, *J. Chem. Phys.*, 1999, **110**, 6158–6170.
- 13 M. Ernzerhof and G. E. Scuseria, *J. Chem. Phys.*, 1999, **110**, 5029–5036.
- 14 E. van Lenthe, E. J. Baerends and J. G. Snijders, *J. Chem. Phys.*, 1993, **99**, 4597–4610.
- 15 E. van Lenthe, E. J. Baerends and J. G. Snijders, *J. Chem. Phys.*, 1994, **101**, 9783–9792.
- 16 E. van Lenthe, R. van Leeuwen, E. J. Baerends and J. G. Snijders, *Int. J. Quantum Chem.*, 1996, **57**, 281–293.
- 17 E. van Lenthe and E. J. Baerends, *J. Comp. Chem.*, 2003, **24**, 1142–1156.